

Multi-Objective Multi-Agent Planning for Discovering and Tracking Unknown and Varying Number of Mobile Objects

Hoa Van Nguyen, Ba-Ngu Vo, Ba-Tuong Vo, Hamid Rezatofighi, and Damith C. Ranasinghe

Abstract—We consider the online planning problem for a team of agents to discover and track an unknown and time-varying number of moving objects from measurements with uncertain measurement-object origins. Since the onboard sensors have limited field of views (FoV), the usual planning strategy based solely on either tracking detected objects or discovering hidden objects is not adequate. We propose a new multi-objective multi-agent partially observable Markov decision process (MM-POMDP) based on information-theoretic criteria and a state-of-the-art online multi-object tracker. The resulting multi-agent planning problem is exponentially complex due to the unknown data association between objects and multi-sensor measurements, and hence, computing an optimal control action is intractable. We prove that the proposed multi-objective value function is a monotone submodular set function, and develop a greedy algorithm that can achieve an 0.5OPT compared to an optimal algorithm. We demonstrate the proposed solution via a series of numerical examples.

Index Terms—Multi-object tracking, random finite sets, multi-agent control, submodular, MM-POMDP.

I. INTRODUCTION

Recent advancements in robotics have inspired transformative applications that use low-cost mobile sensors (*e.g.*, drones or so-called *agents*). These applications range from vision-based surveillance [1]–[4], threat detection via CBRN (chemical, biological, radiological and nuclear) source localisation [5], [6], search and rescue [7], [8], to wildlife monitoring [9]–[12]. At the heart of these applications is Multi-Object Tracking (MOT)—the task of estimating an unknown and time-varying number of objects and their trajectories from sensor measurements. Further, MOT provides awareness of the dynamic environment that the agent operates in, and is fundamental for autonomous operation. A single agent tasked with MOT is limited by its observability, computing resources and energy. Using multiple agents alleviates these problems, improves synergy as well as affording robustness to failures. Realising this potential requires the multiple agents to collaborate and operate autonomously.

Acknowledgement: This work is supported by the Australian Research Council under Linkage Project LP160101177 and LP200301507.

Hoa Van Nguyen and Damith C. Ranasinghe are with the School of Computer Science, The University of Adelaide, SA 5005, Australia (e-mail: {hoavan.nguyen,damith.ranasinghe}@adelaide.edu.au).

Ba-Ngu Vo and Ba-Tuong Vo are with the Department of Electrical and Computer Engineering, Curtin University, Bentley, WA 6102, Australia (e-mail: {ba-nugu.vo,ba-tuong.vo}@curtin.edu.au).

Hamid Rezatofighi is with the Department of Data Science and AI, Monash University, Clayton, VIC 3800, Australia (e-mail: hamid.rezatofighi@monash.edu).

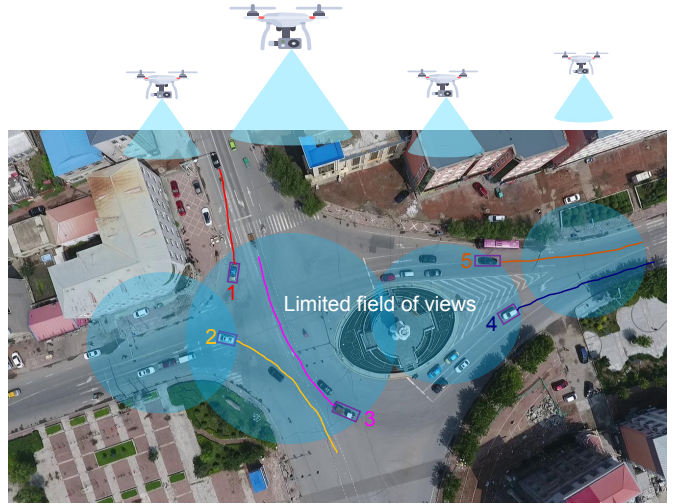


Fig. 1. An example of using a team of multiple unmanned aerial vehicles (UAVs) to search and track multiple cars on the street. The inset images are extracted from the VisDrone-2019 dataset [13].

In this work, we consider the challenging problem of co-ordinating multiple agents to *simultaneously* seek *undetected objects* and track *detected objects*, as illustrated in Fig. 1. Tracking involves estimating the trajectories of the objects and maintaining their provisional identities or labels. Trajectories are important for capturing the behaviour of the objects while labels provide the means for distinguishing individual trajectories and for human/machine users to communicate information on the relevant trajectories. Discovering undetected objects and tracking detected objects are two competing objectives due to the limited field-of-view (FoV) of the sensors (*e.g.* cameras, antenna, and radar) and the random appearance/disappearance of the objects. On one hand, following only the detected objects to track them accurately means that many undetected objects could be missed. On the other hand, leaving detected objects to explore unseen regions for undetected objects will lead to track loss. Thus, the problem of seeking *undetected objects* and tracking *detected objects* is a multi-objective optimisation problem.

Even for standard state-space models, where the system state (and measurement) is a finite-dimensional vector, multi-agent planning with multiple competing objectives is challenging due to complex interactions between agents resulting in combinatorial optimisation problems [14]. In MOT, where the system state (and measurement) is a set of vectors, the problem

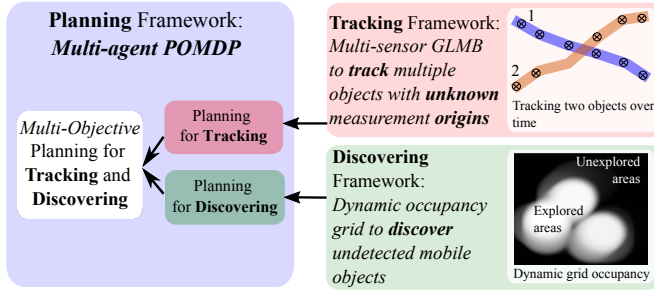


Fig. 2. A schematic for our multi-objective multi-agent planning algorithm.

is further complicated due to: *i*) the unknown and time-varying number of trajectories; *ii*) missing and false detections; and *iii*) unknown data association (object-measurement origin) [15]. Most critically for real-world applications, multi-agent control actions must be computed online and in a timely manner.

Meta-heuristics (so-called bio-inspired) techniques such as genetic algorithms and particle swarm optimisation [16] are prohibitively expensive for real-time applications in dynamic environments such as MOT, especially for multi-agents. Multi-agent planning can be posed as a partially observable Markov decision process (POMDP) [17]–[19], which is gaining significant interests as real-time path planning algorithms [20], [21]. The cooperation problem amongst the agents can be formulated as a decentralised POMDP (Dec-POMDP), whose exact solutions are NEXP-hard [22]. Moreover, for multi-agent POMDPs, the action and observation space grows exponentially with the number of agents [23], and hence not suitable for real-time applications. Distributed POMDP based on distributed constrained optimisation is an still open problem [24]. Moreover, it is intractable in the worst-case(s) [24] [25], which defeats the purpose of distributed operation. So far, the centralised MPOMDP approach [18] offers a more tractable alternative for coordinating multiple agents [26]–[28], and hence, adopted in this work.

The task of computing optimal control actions for multi-agents within POMDP requires a suitable MOT framework that provides a multi-object density as the information state for the POMDP. Hence, amongst various MOT algorithms, we adopt the labelled random finite set (RFS) multi-object filtering framework for its ability to: *i*) conveniently provide the multi-object filtering density (that contains all information on the current set of trajectories); and *ii*) address the time-varying set of labelled trajectories of the mobile objects. Single-agent planning with RFS filters has been studied in with unlimited FoV [29]–[31] for search and track with limited FoV [32], [33], and extended to multi-agent planning using distributed fusion techniques such as generalised covariance intersection (GCI) [28], [34]. However, these multi-agent planning methods are only suitable when the agents have an unlimited detection range [35]. A multi-agent POMDP with an RFS filter was proposed in [27] for searching and localisation, but not tracking.

To achieve the competing detection and tracking objectives as illustrated in Fig. 2, we propose a POMDP with a multi-objective value function consisting of information gains for both detected and undetected objects. A simple solution for

competing objective functions is to weigh and add them together [36]. However, meaningful weighting parameters are difficult to determine. A multi-objective optimisation approach naturally provides a meaningful trade-off between the competing objectives. To the best of our knowledge, multi-agent planning for MOT with a multi-objective value function has not been investigated. The first multi-objective POMDP with RFS filter was proposed in [37] for a sensor selection problem.

For MOT and the computation of the information state, we use the multi-sensor Generalised Labelled Multi-Bernoulli (MS-GLMB) filter [38] which has a *linear* computational complexity with respect to the total number of measurements across the sensors. Further, to reduce the computational time for planning, we propose approximating the differential-entropy-based value function by replacing the information state, which is a GLMB density with a simpler LMB density that matches the first moment and cardinality distribution. We show that the approximate value functions for the POMDP can be computed analytically, thereby enabling the sub-optimal multi-agents control actions to be determined in a timely manner. In summary, the main contributions are:

- 1) a multi-objective POMDP formulation for multi-agent planning to search and track multiple mobile objects;
- 2) an efficient multi-agent path planning algorithm based on differential entropy.

The proposed method is evaluated using the **CRAWDAD taxi dataset** [39] on multi-UAV control for searching and tracking an unknown and time-varying number of taxis in downtown San Francisco, USA. For performance benchmarking, our preliminary work in [40] is used as the ideal or best-case scenarios where data association is known. Tracking errors and computation times of the multi-agent path planning algorithm on ideal scenarios (which can be regarded as a simple special case of our proposed algorithm) serve as performance bounds for realistic scenarios where data association is unknown.

The remainder of this paper is organised as follows. Section II provides relevant background for our Bernoulli-based tracking and planning framework. Section III presents our proposed multi-objective value function to control multi-agents for simultaneously tracking and discovering objects. Section IV evaluates our proposed method on a real-world dataset. Section V summarises our contributions and discusses future directions.

II. BACKGROUND

This section presents the problem statement, as well as the necessary background on random finite sets with Bayesian estimation, the MS-GLMB filter and MPOMDP.

A. Problem statement

Consider a team of agents, identified by a set of unique labels $\mathcal{N} = \{1, \dots, |\mathcal{N}|\}$, monitoring a spatial area $G \subset \mathbb{R}^{d_x}$ to search and track a time-varying and unknown number of moving objects. The agents can self-localise (*e.g.*, using its on-board GPS sensors) and are equipped with range-limited and homogeneous sensors that register measurements with *unknown data associations* (*i.e.*, the measurement-to-object

origin is unknown). The agents can communicate to a central node (*e.g.*, send measurements to a central node for processing), while the central node can compute and send control actions to the agents [27], [29]. We assume that conditional on the ensemble of object states, the measurements obtained by individual agents are independent [36], [41]¹.

Throughout, we follow the notation used in [42]. Lowercase letters (*e.g.*, x, \mathbf{x}) denote the state vectors of individual objects, referred to as single-object states. States augmented with labels are bolded to distinguish them from unlabelled ones. Uppercase letters (*e.g.*, X, \mathbf{X}) denote sets of single-object states at a given time, referred to as multi-object states. Spaces and labelled spaces are denoted by blackboard uppercase letters (*e.g.*, \mathbb{X}, \mathbb{L}) and bold blackboard uppercase letters (*e.g.*, $\mathbf{\mathbb{X}}, \mathbf{\mathbb{U}}$), respectively. For a given set S , $\mathcal{F}(S)$, $|S|$, $1_S(\cdot)$, $\delta_S[\cdot]$ denote, respectively, the class of finite subsets, cardinality, indicator function, and (generalised) Kronecker delta function, of S ($\delta_S[X] = 1$, if $X = S$, and zero otherwise). For a given function f , its multi-object exponential f^X is defined as $\prod_{x \in X} f(x)$, with $f^\emptyset = 0$. The inner product $\int f(x)g(x)dx$ is written as $\langle f, g \rangle$.

B. Bayesian Multi-object Estimation

A POMDP formulation models the *system state* as a random variable, and requires an *information state* that captures all information pertaining to the system state at each instant. The system state in our multi-agent path planning problem is the set \mathbf{X} of labelled states of the objects at each instant, herein referred to as the *multi-object state*. The cardinality (number of elements) of \mathbf{X} varies with time due to the appearance and disappearance of objects from one instant to the next. Each element of \mathbf{X} is an ordered pair $\mathbf{x} = (x, \ell)$, where x is a state vector in some finite dimensional state space \mathbb{X} , and ℓ is a unique label in some discrete label space \mathbb{L} , fixed for the lifetime of the object, and consists of the object's time of birth and an index to distinguish those born at the same time [43]. We denote $\mathcal{L}(\mathbf{x})$ as the label of $\mathbf{x} \in \mathbb{X} \times \mathbb{L}$, $\mathcal{L}(\mathbf{X}) \triangleq \{\mathcal{L}(\mathbf{x}) : \mathbf{x} \in \mathbf{X}\}$ for any finite $\mathbf{X} \subset \mathbb{X} \times \mathbb{L}$, and $\Delta(\mathbf{X}) \triangleq \delta_{|\mathbf{X}|}[[\mathcal{L}(\mathbf{X})]]$ as the *distinct label indicator*. At any time, the multi-object state \mathbf{X} must have distinct labels, *i.e.* $\Delta(\mathbf{X}) = 1$. Hence, the *trajectory* of an object is a sequence of consecutive states with a common label [43].

A random finite set (RFS) model [44] succinctly captures the random nature of the multi-object state, and also provides its probability density as the information state for the POMDP. An RFS X of a state-space \mathbb{X} is a random variable taking values in $\mathcal{F}(\mathbb{X})$, and is commonly characterised by Mahler's multi-object density [15], [44] (see also subsection II-C). Since the elements of multi-object states in this work are distinctly labelled, we use a *labelled RFS* model. Given an RFS X of \mathbb{X} and a (discrete) label space \mathbb{L} , a labelled RFS \mathbf{X} is an RFS of $\mathbf{\mathbb{X}} \triangleq \mathbb{X} \times \mathbb{L}$ constructed by marking the elements of X with distinct labels from \mathbb{L} [43].

In a Bayesian filtering context, the (labelled) multi-object filtering density at the current time k (conditioned the obser-

vation history up to time k) contains all information on the ensemble of states and their trajectories [43]. For compactness, the subscript k for the current time is omitted, and the next time $k+1$ is denoted by $+$. Analogous to the standard Bayes filter, the multi-object filtering density is propagated forward in time via the multi-object Bayes filter [15]

$$\pi_+(\mathbf{X}_+) \propto g(Z_+ | \mathbf{X}_+) \int f_+(\mathbf{X}_+ | \mathbf{X}) \pi(\mathbf{X}) \delta \mathbf{X}, \quad (1)$$

where: π , π_+ and \mathbf{X} , \mathbf{X}_+ are the multi-object filtering densities and multi-object states at the current and next times; g and f_+ are the multi-object observation likelihood and transition density; and the integral is Mahler's set integral. The multi-object observation likelihood g captures the detections, false alarms, occlusions, and misdetections. The multi-object transition density f_+ captures the motions as well as births and deaths of objects.

C. Generalized Labeled Multi-Bernoulli Filtering

At time k , an object with state $\mathbf{x} = (x, \ell) \in \mathbf{X}$ either survives with probability $P_S(\mathbf{x})$ or dies with probability $1 - P_S(\mathbf{x})$ [43]. Conditional on survival it evolves to state $\mathbf{x}_+ = (x_+, \ell_+)$ at the next time according to the transition density $f_{S,+}(x_+ | x, \ell) \delta_\ell[\ell_+]$, where $\delta_\ell[\ell_+]$ ensures it retains the same label. In addition, an object with state $\mathbf{x}_+ = (x_+, \ell_+)$ is born at time $k+1$ with probability $P_{B,+}(\ell_+)$, and its unlabelled state x_+ is distributed according to the probability density $f_{B,+}(\cdot, \ell)$. It is standard practice to assume that, conditional on the current multi-object state, objects are born or displaced at the next time, independently of one another [15].

For an agent with label $n \in \mathcal{N}$, we denote $\mathbf{U}^{(n)} \triangleq \mathbb{U} \times \{n\}$, $\mathbf{A}^{(n)} \triangleq \mathbb{A} \times \{n\}$, and $\mathbf{Z}^{(n)} \triangleq \mathbb{Z} \times \{n\}$. For simplicity, assume that all agents have the same common agent-state space² $\mathbf{U} \triangleq \mathbb{U} \times \mathcal{N}$, a common discrete control action space $\mathbf{A} \triangleq \mathbb{A} \times \mathcal{N}$ (*e.g.*, $\mathbb{A} = \{\rightarrow, \searrow, \downarrow, \swarrow, \leftarrow, \nwarrow, \uparrow, \nearrow\}$), and a common measurement space (homogenous sensors) $\mathbf{Z} \triangleq \mathbb{Z} \times \mathcal{N}$. Given a set \mathbf{X} of objects, each $\mathbf{x} \in \mathbf{X}$ has probability $P_D(\mathbf{x}, \mathbf{u})$ of being detected by an agent with state $\mathbf{u} = (u, n) \in \mathbf{U}$, and generates an observation $\mathbf{z} = (z, n') \in \mathbf{Z}$ with measurement likelihood [45]:

$$g(\mathbf{z} | \mathbf{x}, \mathbf{u}) = \delta_n[n'] g(z | \mathbf{x}, u, n) = \delta_n[n'] g^{(n)}(z | \mathbf{x}, u), \quad (2)$$

or missed with probability $1 - P_D(\mathbf{x}, \mathbf{u})$. The term $\delta_n[n']$ ensures that measurements generated by agent (with label) n are tagged with the same label. The observation set $\mathbf{Z}^{(n)} = \{(z_1, n), \dots, (z_{|\mathbf{Z}^{(n)}|}, n)\} \in \mathcal{F}(\mathbf{Z})$ at agent n , is formed by the superposition of the (object-originated) detections and Poisson clutter with intensity $\kappa(\mathbf{z} | \mathbf{u}) = \delta_n[n'] \kappa(z | u, n) = \delta_n[n'] \kappa^{(n)}(z | u)$. It is standard practice to assume that conditional on \mathbf{X} , detections are independent of each other and clutter [44], and that the measurements obtained by individual agents are independent [36], [41]. The multi-agent observation can be expressed as the disjoint union $\mathbf{Z} \triangleq \mathbf{Z}^{(1)} \uplus \dots \uplus \mathbf{Z}^{(|\mathcal{N}|)} \in \mathcal{F}(\mathbf{Z})$ or equivalently as the array $\mathbf{Z} \triangleq (\mathbf{Z}^{(1)}, \dots, \mathbf{Z}^{(|\mathcal{N}|)})$.

¹This assumption holds if there is no interference among agents when getting measurements.

²We assume that the measurement errors collected from agents' internal actuator-sensor are negligible, thus the agent state is completely known.

Remark 1. The detection probability, the clutter rate and the measurement likelihood always depend on the agent-state u . For notational simplicity, u will usually be suppressed unless otherwise stated, *i.e.*, $P_D(\mathbf{x}, u, n) \triangleq P_D^{(n)}(\mathbf{x})$, $\kappa(z, n|u, n) \triangleq \kappa^{(n)}(z)$, and $g(z, n|\mathbf{x}, u, n) \triangleq g^{(n)}(z|\mathbf{x})$.

The objects are mapped to the multi-agent observation by a multi-agent *association map* γ , where individual elements in $\mathbf{Z}^{(n)}$ are associated with objects via the *positive 1-1 map*³ $\gamma^{(n)} : \mathbb{L} \rightarrow \{-1: |\mathbf{Z}^{(n)}|\}$, and $\gamma^{(1)}(\ell) = \dots = \gamma^{(|\mathcal{N}|)}(\ell) = -1$ if ℓ is a dead/unborn label [38]. Here $\gamma^{(n)}(\ell) = -1$ means object ℓ does not exist, $\gamma^{(n)}(\ell) = 0$ means object ℓ is not detected by agent n , and $\gamma^{(n)}(\ell) > 0$ means object ℓ generates observation $\mathbf{z}_{\gamma^{(n)}(\ell)}$ at agent n [43]. The positive 1-1 property ensures each observation from agent n originates from at most one object, and the set $\mathcal{L}(\gamma) \triangleq \{\ell \in \mathbb{L} : \gamma^{(1)}(\ell), \dots, \gamma^{(|\mathcal{N}|)}(\ell) \geq 0\}$ is called the *live labels* of γ . The space of all such multi-agent association is denoted as Γ .

The Bayes recursion (1) admits an analytical filtering density in the form of a Generalised Labelled Multi-Bernoulli (GLMB) [43]:

$$\pi(\mathbf{X}) = \Delta(\mathbf{X}) \sum_{I, \xi} w^{(I, \xi)} \delta_I[\mathcal{L}(\mathbf{X})] \left[p^{(\xi)} \right]^{\mathbf{X}}, \quad (3)$$

where $I \in \mathcal{F}(\mathbb{L})$, $\xi \triangleq \gamma_{1:k} \in \Xi$, the space of all (multi-agent) association histories up to the current time, each $w^{(I, \xi)}$ is non-negative such that $\sum_{I, \xi} w^{(I, \xi)} = 1$, and each $p^{(\xi)}(\cdot, \ell)$ is a probability density on \mathbb{X} . For convenience, a GLMB is represented by the set of components

$$\pi \triangleq \left\{ \left(w^{(I, \xi)}, p^{(\xi)} \right) : (I, \xi) \in \mathcal{F}(\mathbb{L}) \times \Xi \right\}. \quad (4)$$

Under the standard multi-object system model, if the current filtering density is the GLMB (4), then the filtering density at the next time is a GLMB given by the *MS-GLMB recursion* [46]

$$\pi_+ = \Omega(\pi; \mathbf{Z}_+). \quad (5)$$

The actual mathematical expression for the operator $\Omega(\cdot; \mathbf{Z}_+)$: $\pi \mapsto \pi_+$ is provided in Appendix A. Consequently, if the initial prior is a GLMB, then all subsequent filtering densities are GLMBs. Note that Ω also depends on the model parameters for birth $P_{B,+}$, $f_{B,+}$, death/survival P_S , motion $f_{S,+}$, false alarms $\kappa_+^{(1)}, \dots, \kappa_+^{(|\mathcal{N}|)}$, detection probabilities $P_{D,+}^{(1)}, \dots, P_{D,+}^{(|\mathcal{N}|)}$, and (single-object) observation likelihoods $g_+^{(1)}, \dots, g_+^{(|\mathcal{N}|)}$.

A GLMB density $\pi(\cdot)$ can be approximated by an LMB $\hat{\pi}(\cdot)$ with the same moment and cardinality distribution [47], given by:

$$\hat{\pi}(\mathbf{X}) = \Delta(\mathbf{X}) [1 - r^{(\cdot)}]^{\mathbb{L} - \mathcal{L}(\mathbf{X})} r^{\mathcal{L}(\mathbf{X})} p^{\mathbf{X}}, \quad (6)$$

where

$$r^{(\ell)} = \sum_{(I, \xi) \in \mathcal{F}(\mathbb{L}) \times \Xi} 1_I(\ell) w^{(I, \xi)}, \quad (7)$$

$$p^{(\ell)}(x) = \frac{1}{r^{(\ell)}} \sum_{(I, \xi) \in \mathcal{F}(\mathbb{L}) \times \Xi} 1_I(\ell) w^{(I, \xi)} p^{(\xi)}(x, \ell) \quad (8)$$

³No two distinct arguments are mapped to the same positive value.

are, respectively, the existence probability of object ℓ , and its the probability density. An LMB is completely characterised by the parameter set $\{r^{(\ell)}, p^{(\ell)}(\cdot)\}_{\ell \in \mathbb{L}}$

D. Multi-agent POMDP (MPOMDP)

A partition matroid of the action space $\mathbf{A}^{(n)}$ is a collection of subsets of $\mathbf{A}^{(n)}$, defined by [48]:

$$\mathcal{M} = \{A \subseteq \mathbf{A} : |A \cap \mathbf{A}^{(n)}| \leq 1 \ \forall n \in \mathcal{N}\}. \quad (9)$$

A set A of actions with $|A \cap \mathbf{A}^{(n)}| = 1$ is said to be complete for agent n . If $|A \cap \mathbf{A}^{(n)}| = 0$ then A is said to be incomplete for agent n . The partition matroid construct ensures that each agent n can only select at *most* one control action from its local control action space $\mathbf{A}^{(n)}$.

A centralised multi-agent POMDP for tracking multi-objects can be characterised by the tuple $(\mathcal{N}, H, \mathcal{F}(\mathbf{X}), \mathcal{F}(\mathbf{Z}), \mathcal{F}(\mathbf{U}), \mathcal{M}, f_+, g, \rho)$, where:

- \mathcal{N} is the finite set of agent labels;
- H is the look-ahead time horizon;
- $\mathcal{F}(\mathbf{X})$ is the labelled multi-object state space;
- $\mathcal{F}(\mathbf{Z})$ is the common observation space of the all agents (assumed to have homogeneous sensors);
- $\mathcal{F}(\mathbf{U})$ is the common state space of all agents;
- \mathcal{M} is the partition matroid of all actions of all agents;
- $f_+ : [\mathcal{F}(\mathbf{X}) \times \mathcal{F}(\mathbf{U})] \times [\mathcal{F}(\mathbf{X}) \times \mathcal{F}(\mathbf{U})] \times \mathcal{M} \rightarrow [0, 1]$ defines the transition kernel $f_+((\mathbf{X}_+, \mathbf{U}_+)|(\mathbf{X}, \mathbf{U}), A)$;
- $g : \mathcal{F}(\mathbf{Z}) \times [\mathcal{F}(\mathbf{X}) \times \mathcal{F}(\mathbf{U})] \times \mathcal{M} \rightarrow [0, 1]$ defines the joint observation likelihood function $g(\mathbf{Z}_+(A)|(\mathbf{X}_+, \mathbf{U}_+(A)), A)$;
- $\rho : [\mathcal{F}(\mathbf{X}) \times \mathcal{F}(\mathbf{U})] \times \mathcal{M} \times \mathcal{F}(\mathbf{Z}) \rightarrow \mathbb{R}$ defines the immediate reward $\rho((\mathbf{X}, \mathbf{U}(A)), A, \mathbf{Z}(A))$ for being in state $(\mathbf{X}, \mathbf{U}(A))$ after performing action $A \in \mathcal{M}$ which results in measurement $\mathbf{Z}(A)$.

The coordination of the agents is accomplished via the control action $A \in \mathcal{M}$. Each $\mathbf{a}^{(n)} \in A$ at time k prescribes a trajectory $\mathbf{u}_{1:H}(\mathbf{a}^{(n)}) \triangleq (\mathbf{u}_{k+1}(\mathbf{a}^{(n)}), \dots, \mathbf{u}_{k+H}(\mathbf{a}^{(n)}))$ comprising of positions for agent n on the interval $\{k+1, \dots, k+H\}$, along which it collects the multi-object measurement history $\mathbf{Z}_{1:H}(\mathbf{a}^{(n)}) \triangleq (\mathbf{Z}_{k+1}(\mathbf{a}^{(n)}), \dots, \mathbf{Z}_{k+H}(\mathbf{a}^{(n)}))$. For notational convenience, we denote

$$\mathbf{X}_{1:H} \triangleq (\mathbf{X}_{k+1}, \dots, \mathbf{X}_{k+H}), \quad (10)$$

$$\mathbf{U}_{1:H}(A) \triangleq (\mathbf{U}_{k+1}(A), \dots, \mathbf{U}_{k+H}(A)), \quad (11)$$

$$\mathbf{Z}_{1:H}(A) \triangleq (\mathbf{Z}_{k+1}(A), \dots, \mathbf{Z}_{k+H}(A)), \quad (12)$$

where $\forall j \in \{k+1, \dots, k+H\}$:

$$\mathbf{U}_j(A) \triangleq \uplus_{\mathbf{a} \in A} \mathbf{u}_j(\mathbf{a}), \quad (13)$$

$$\mathbf{Z}_j(A) \triangleq \uplus_{\mathbf{a} \in A} \mathbf{Z}_j(\mathbf{a}). \quad (14)$$

A POMDP seeks, at time k , the control action(s) $\mathbf{A} \in \mathcal{M}$ that maximises the the *value function*:

$$V(\mathbf{X}_{1:H}, \mathbf{U}_{1:H}(\mathbf{A}), \mathbf{A}, \mathbf{Z}_{1:H}(\mathbf{A})) \triangleq \mathbb{E} \left[\sum_{j=k+1}^{k+H} \varrho(\mathbf{X}_j, \mathbf{U}_j(\mathbf{A}), \mathbf{A}, \mathbf{Z}_j(\mathbf{A})) \right], \quad (15)$$

which is the expected sum of immediate rewards $\varrho(\cdot)$ over horizon H . Here, $\mathbb{E}[\cdot]$ denotes the expected operator.

Remark 2. Notably, the value function $V(\cdot)$ always depends on the agents' positions \mathbf{U} and action \mathbf{A} . Hereafter, for notational simplicity, \mathbf{U} and \mathbf{A} are suppressed, *e.g.*, $V(\mathbf{X}_{1:H}, \mathbf{U}_{1:H}(\mathbf{A}), \mathbf{A}, \mathbf{Z}_{1:H}(\mathbf{A})) \triangleq V(\mathbf{X}_{1:H}, \mathbf{Z}_{1:H}(\mathbf{A}))$; $\varrho(\mathbf{X}_j, \mathbf{U}_j(\mathbf{A}), \mathbf{A}, \mathbf{Z}_j(\mathbf{A})) \triangleq \varrho(\mathbf{X}_j, \mathbf{Z}_j(\mathbf{A}))$.

In general, analytic solutions to POMDP in (15) are not available while numerical solutions (*e.g.*, using Monte Carlo integration in [10], [29] are computationally intractable/intensive, especially for multiple agents. Alternatively, a computationally tractable value-function based on the notion of predicted ideal measurement set (PIMS) was proposed in [49], *i.e.*,

$$V(\mathbf{X}_{1:H}, \widehat{\mathbf{Z}}_{1:H}(\mathbf{A})) = \sum_{j=k+1}^{k+H} \varrho(\mathbf{X}_j, \widehat{\mathbf{Z}}_j(\mathbf{A})). \quad (16)$$

where the predicted ideal measurement set $\widehat{\mathbf{Z}}_j(\mathbf{A})$ is constructed by generating measurements from the predicted multi-object state without measurement noise, clutter nor misdetection. When no confusion arises, we denote $V(\mathbf{X}_{1:H}, \widehat{\mathbf{Z}}_{1:H}(\mathbf{A}))$ as $V(\mathbf{A})$.

III. PLANNING FOR TRACKING AND DISCOVERING MULTIPLE OBJECTS

This section presents our solution to the problem of manoeuvring multiple agents with limited FoV sensors to search, detect and track an unknown and time-varying number of objects. This problem is very challenging due to: *i*) the undetected objects resulting from the limited FoVs; *ii*) the unknown locations of objects without any prior information; *iii*) the complex data association problem due to unknown measurement-object origins as well as an unknown and time-varying number of objects; and *iv*) the combinatorial nature in computing the control actions for multiple agents. An overview of the proposed solution is illustrated in Fig. 2.

We begin by introducing the concepts of differential entropy and mutual information in subsection III-A, which are instrumental for formulating the value function. As depicted in Fig. 2, the considered problem requires computing the optimal control action for multi-agents to achieve the competing objectives: *i*) *tracking detected objects*, and *ii*) *discovering (searching) mobile undetected objects* due to limited FoV. On the one hand, we address the **first** objective, *i.e.*, *planning for tracking*, by: a) utilising the MS-GLMB filter (see subsection II-C) to track an unknown and time-varying number of objects; and b) computing the optimal control action to *track* multiple objects

via a new closed-form expression of mutual information for LMB densities in subsection III-B. On the other hand, we address the **second** objective, *i.e.*, *planning for discovering*, by a) using an occupancy grid to estimate the discovery probability (*i.e.*, the probability that at least one undetected mobile object occupies the grid cells) in subsection III-C1; and b) computing the optimal control action based on the mutual information of the occupancy grid to *discover* (search) undetected mobile objects, in subsection III-C2.

In subsection 3.4, to accommodate the competing objectives, we seek the multi-agent control actions that *simultaneously optimise the tracking of detected objects and the discovering of undetected objects* to achieve a Pareto solution set, *i.e.*, solutions such that no individual solution can improve one objective without degrading at least one of the remaining objectives. Lastly, since computing the optimal control action for multi-agents is a combinatorial problem, we propose a greedy search algorithm with a performance bound in subsection III-E.

A. Differential Entropy and Mutual Information

In this subsection, we extend the concepts of differential entropy [50, pp.243], and mutual information [50, pp.251] to RFS. Differential entropy is commonly used to measure information uncertainty while and mutual information commonly used to measure the information content of one random variable in another. These concepts are needed to formulate the objectives for our multi-agent POMDP, as well as the derivation of tractable solutions. To define meaningful differential entropy and mutual information for RFS, we need to take a closer look at the notion of probability density for RFS.

The probability density $f : \mathcal{F}(\mathbb{X}) \rightarrow [0, \infty)$, of an RFS X , is usually taken with respect to the dominating measure μ defined for each measurable $\mathcal{T} \subseteq \mathcal{F}(\mathbb{X})$ by (see *e.g.*, [51], [52]):

$$\mu(\mathcal{T}) = \sum_{i=0}^{\infty} \frac{1}{i!K^i} \int 1_{\mathcal{T}}(\{x_1, \dots, x_i\}) d(x_1, \dots, x_i),$$

where K is the unit of hyper-volume on \mathbb{X} , $1_{\mathcal{T}}(\cdot)$ is the indicator function for \mathcal{T} , and by convention the integral for $i = 0$ is $1_{\mathcal{T}}(\emptyset)$. Note that the probability density f and the reference measure μ are unitless. The role of μ is analogous to the Lebesgue measure on \mathbb{X} , and the integral of a function $f : \mathcal{F}(\mathbb{X}) \rightarrow (-\infty, \infty)$ with respect to μ , given by

$$\int f(X) \mu(dX) = \sum_{i=0}^{\infty} \frac{1}{i!K^i} \int f(\{x_1, \dots, x_i\}) d(x_1, \dots, x_i).$$

Note that this integral is equivalent to Mahler's set integral [44], defined for a function π by

$$\int \pi(X) \delta X = \sum_{i=0}^{\infty} \frac{1}{i!} \int \pi(\{x_1, \dots, x_i\}) d(x_1, \dots, x_i),$$

in the sense that $\int K^{-|X|} f(X) \delta X = \int f(X) \mu(dX)$. Hence, $K^{-|X|} f(X)$ is Mahler's Finite Set Statistics (FISST) density (see [53]).

Analogous to random variables, differential entropy and mutual information for RFS are defined as follows.

Definition 1. The differential entropy $h(X)$ of a random finite set X , described by a probability density f_X , is defined as

$$h(X) = - \int f_X(Y) \log(f_X(Y)) \mu(dY). \quad (17)$$

Remark 3. Using the equivalence with Mahler's set integral, the differential entropy of an RFS X with Finite Set Statistics (FISST) density π_X can be written as

$$h(X) = - \int \pi_X(Y) \log(K^{|Y|} \pi_X(Y)) \delta Y. \quad (18)$$

Definition 2. The mutual information between the RFSs X and Z is defined as

$$I(X; Z) = h(X) - h(X|Z), \quad (19)$$

where

$$h(X|Z) = \int h(X|Z = \zeta) \pi_Z(\zeta) \delta \zeta, \quad (20)$$

and $\pi_Z(\cdot)$ is the (FISST) density of Z .

For an LMB RFS, see (6), the differential entropy can be expressed analytically as follows (the proof is given in Appendix C).

Proposition 1. The differential entropy of an LMB X , with parameter set $\{r^{(\ell)}, p^{(\ell)}(\cdot)\}_{\ell \in \mathbb{L}}$ is

$$\begin{aligned} h(X) &= - \sum_{L \subseteq \mathbb{L}} w(L) \log w(L) \\ &\quad - \sum_{\emptyset \neq L \subseteq \mathbb{L}} w(L) \left(\sum_{\ell \in L} \langle p^{(\ell)}, \log(Kp^{(\ell)}) \rangle \right). \end{aligned} \quad (21)$$

where $w(L) = [1 - r^{(\cdot)}]^{\mathbb{L} - L} [r^{(\cdot)}]^L$.

Note that if each single-object density is a Gaussian mixture (*i.e.*, $p^{(\ell)}(x) = \sum_{i=1}^{N_\ell} \alpha_i^{(\ell)} \mathcal{G}(x; m_i^{(\ell)}, \Sigma_i^{(\ell)})$, then we can approximate $p^{(\ell)}(x) \approx \mathcal{G}(x; \bar{m}^{(\ell)}, \bar{\Sigma}^{(\ell)})$ as in [54]:

$$\begin{aligned} \bar{m}^{(\ell)} &= \sum_{i=1}^{N_\ell} \alpha_i^{(\ell)} m_i^{(\ell)}, \\ \bar{\Sigma}^{(\ell)} &= \sum_{i=1}^{N_\ell} \alpha_i^{(\ell)} \left[\Sigma_i^{(\ell)} + (m_i^{(\ell)} - \bar{m}^{(\ell)}) (m_i^{(\ell)} - \bar{m}^{(\ell)})^T \right]. \end{aligned}$$

Consequently, we have:

$$-\int p^{(\ell)}(x) \log [Kp^{(\ell)}(x)] dx \approx \frac{1}{2} \log \left[\det(2\pi e \bar{\Sigma}^{(\ell)}) \right],$$

and (21) can be approximated as:

$$\begin{aligned} h(X) &\approx - \sum_{L \subseteq \mathbb{L}} w(L) \log(w(L)) \\ &\quad + \frac{1}{2} \sum_{\emptyset \neq L \subseteq \mathbb{L}} w(L) \sum_{\ell \in L} \left(\log \left[\det(2\pi e \bar{\Sigma}^{(\ell)}) \right] \right). \end{aligned} \quad (22)$$

Remark 4. A special case of the above proposition is the differential entropy of a Bernoulli RFS, *i.e.* an LMB with only one component, parameterised by (r, p) :

$$h(X) = -(1 - r) \log(1 - r) - r \log(r) - \langle p^{(\ell)}, \log(Kp^{(\ell)}) \rangle.$$

Optimising the value function of a realistic POMDP is computationally intensive if not intractable. Fortunately, when the value function is a *monotone submodular* set function, sub-optimal solutions can be computed using a greedy algorithm with drastically lower complexity. In the following we establish monotone submodularity of mutual information, see proof in Appendix C.

Definition 3. [55]. A set function $q : \mathcal{F}(\mathbb{A}) \rightarrow \mathbb{R}$, *i.e.* a real-valued function whose domain is the class of finite subsets of a given set, is said to be *monotone* if $q(\mathbf{A}) \leq q(\mathbf{B}) \forall \mathbf{A} \subseteq \mathbf{B} \subseteq \mathbb{A}$, and *submodular* if $q(\mathbf{B} \cup \{\mathbf{a}\}) - q(\mathbf{B}) \leq q(\mathbf{A} \cup \{\mathbf{a}\}) - q(\mathbf{A})$, $\forall \mathbf{A} \subseteq \mathbf{B} \subseteq \mathbb{A}, \forall \mathbf{a} \in \mathbb{A} \setminus \mathbf{B}$.

Proposition 2. Suppose that conditioned on the multi-object state, the measurements collected by the agents are conditionally independent from each other. Given a set $\mathbf{A} \in \mathcal{F}(\mathbb{A})$ of actions, let $q_I(\mathbf{A}) \triangleq I(\mathbf{X}; \mathbf{Z}(\mathbf{A}))$ denote the mutual information between the multi-object state \mathbf{X} (with density π_X) and measurement $\mathbf{Z}(\mathbf{A})$ (with density $\pi_{\mathbf{Z}(\mathbf{A})}$) collected by the agents when the actions in \mathbf{A} are taken. Then $q_I(\cdot)$ is a monotone submodular set function on $\mathcal{F}(\mathbb{A})$.

B. Planning for tracking

This subsection presents our information-based tracking value function to accurately track the detected object by reducing the overall estimation uncertainty. Notably, it is not necessary to define a value function with the expected operator as in (15). In this work, inspired by the PIMS approach in [49] (see (16)), we propose using a novel value function via the mutual information $I(\mathbf{X}; \widehat{\mathbf{Z}})$ between the multi-object state \mathbf{X} and the *ideal* measurement state $\widehat{\mathbf{Z}}$. Here, $\widehat{\mathbf{Z}}$ is generated from \mathbf{X} without data association (*i.e.*, known as the measurement-object assignment), as well as without measurement noise, clutters or misdetections. The value function is defined as

$$V_1(\mathbf{A}) = \sum_{j=k+1}^{k+H} I(\mathbf{X}_j; \widehat{\mathbf{Z}}_j(\mathbf{A})), \quad (23)$$

where $I(\mathbf{X}; \widehat{\mathbf{Z}}) = h(\mathbf{X}) - h(\mathbf{X}|\widehat{\mathbf{Z}})$ and $h(\cdot)$ defined in (21).

Corollary 3. The value function $V_1(\mathbf{A})$ in (23) is a monotone submodular set function.

Proof. From Proposition 2, $I(\mathbf{X}; \widehat{\mathbf{Z}}(\mathbf{A}))$ is a monotone submodular set function and $V_1(\mathbf{A})$ is a positive linear combination of it. Hence, it follows from [55, pp.272], $V_1(\mathbf{A})$ is a monotone submodular set function. \square

C. Planning for discovery

1) *Occupancy grid for undetected objects.*: Some objects of interest can be outside of the sensor's limited FoVs, and thus cannot be detected. However, the knowledge of undetected objects outside the sensor's FoVs is usually not exploited. In this

work, we develop an occupancy grid to capture the knowledge about undetected objects outside sensor's FoV. Intuitively, the knowledge of unexplored regions can be incorporated in the planning to increase the likelihood of discovering new objects.

In contrast to *static* occupancy grids for *stationary* objects in [36], [41], a *dynamic* occupancy grid is proposed by including the probability of each grid cell containing at least one undetected *mobile* object, namely the *discovery probability*. In particular, we divide the search area of interest G into an occupancy grid, *i.e.*, $G = \kappa^{(1)} \cup \dots \cup \kappa^{(N_\kappa)} \subset \mathbb{R}^{d_\kappa}$. Further, we define a pair $(r_\kappa^{(i)}, \kappa_c^{(i)})$ to be associated with $\kappa^{(i)}$ such that $\kappa_c^{(i)} \in \kappa^{(i)}$ denotes the centre point of cell $\kappa^{(i)}$, and $r_\kappa^{(i)} \in [0, 1]$ denotes the discovery probability, *i.e.* the probability that the occupancy cell $\kappa^{(i)}$ contains at least one *undetected mobile object*.

For any cell $\kappa^{(i)} \subset G$, since undetected objects may or may not be present in $\kappa^{(i)}$, we model the occupancy state in cell $\kappa^{(i)}$ by the Bernoulli RFS $X^{(i)}$ whose state can be either \emptyset or $\{\kappa_c^{(i)}\}$. When $X^{(i)}$ is empty, it is *not* occupied with probability $1 - r_\kappa^{(i)}$. When $X^{(i)}$ is not empty, it is occupied (by undetected objects) with probability $r_\kappa^{(i)}$. The density of the Bernoulli RFS $X^{(i)}$ is given by

$$\pi(X^{(i)}) = \begin{cases} 1 - r_\kappa^{(i)}, & \text{if } X^{(i)} = \emptyset, \\ r_\kappa^{(i)}, & \text{if } X^{(i)} = \{\kappa_c^{(i)}\}. \end{cases} \quad (24)$$

Thus, the problem of computing the grid occupancy of undetected objects in cell $\kappa^{(i)}$ is equivalent to that of tracking a stationary object located at the centroid of cell $\kappa_c^{(i)}$, wherein our goal is to determine the probability $r_\kappa^{(i)}$. Hence, we apply the multi-sensor Bernoulli filter (MS-BF) in [56] to compute $r_\kappa^{(i)}$ over time using *the empty measurements*⁴. Specially, suppose $r_\kappa^{(i)}$ and $r_{\kappa,+}^{(i)}$ are the probability at time k and $k+1$ respectively, we have:

$$r_{\kappa,+}^{(i)} = \Psi^{(|\mathcal{N}|)} \circ \dots \circ \Psi^{(1)}(r_{\kappa,B}^{(i)}(1 - r_\kappa^{(i)}) + r_\kappa^{(i)} P_s(\kappa_c^{(i)})). \quad (25)$$

Here

$$[\Psi^{(n)}(r_\kappa^{(i)})] = \frac{(1 - P_{D,+}^{(n)}(\kappa_c^{(i)}))r_\kappa^{(i)}}{1 - r_\kappa^{(i)} + r_\kappa^{(i)}(1 - P_{D,+}^{(n)}(\kappa_c^{(i)}))}, \quad (26)$$

where $P_S(\cdot)$ and $P_{D,+}^{(n)}(\cdot)$ are the same survival and detection probabilities defined in subsection II-C, $r_{\kappa,B}^{(i)}$ is the birth probability, *i.e.* the probability of undetected objects appear/enter the cell $\kappa^{(i)}$. At initial time $k = 0$, we can set $r_{\kappa,0}^{(i)} = r_{\kappa,B}^{(i)}$ if there is no prior information. Notably, from (25) and (26), we can see that the discovery probability $r_\kappa^{(i)}$ depends on the detection probability $P_{D,+}^{(n)}(\kappa_c^{(i)})$ —a function of the location of sensor n (see Remark 1) and the centre point $\kappa_c^{(i)}$ —which conforms with our intuition.

2) *Planning for discovery*: This subsection presents our information-based discovering value function to increase agents' chances to detect undetected objects. The suggested value function focuses on maximising the mutual information

⁴Since objects are undetected, the measurements from the undetected objects are empty.

amongst the occupancy grid cells G and the empty measurement set Z_j^\emptyset . Since the measurement set is empty, the expected operator in (15) no longer has an effect, *i.e.*,

$$V_2(\mathbf{A}) = \sum_{j=k+1}^{k+H} I(G_k; Z_j^\emptyset(\mathbf{A})), \quad (27)$$

where $I(G_k; Z_j^\emptyset(\mathbf{A})) = \mathcal{H}(G_k) - \mathcal{H}(G_k|Z_j^\emptyset(\mathbf{A}))$, $\mathcal{H}(G_k)$ is the Shannon entropy (a discrete version of differential entropy $h(\cdot)$) of G_k . Because each grid cell $\kappa^{(i)}$ is associated with Bernoulli random variable while its spatial density is unity, according to Remark 4, we have:

$$\mathcal{H}(G_k) = - \sum_{i=1}^{N_\kappa} [r_{\kappa,k}^{(i)} \log(r_{\kappa,k}^{(i)}) + (1 - r_{\kappa,k}^{(i)}) \log(1 - r_{\kappa,k}^{(i)})], \quad (28)$$

and $\mathcal{H}(G_k|Z_j^\emptyset(\mathbf{a}))$ follows the exact form as in (28) where $r_{\kappa,j}^{(i)}$ is computed by propagating $r_{\kappa,k}^{(i)}$ from k to j using (25) with the *empty measurement* $Z_j^\emptyset(\mathbf{A})$.

Proposition 4. The value function V_2 in (27) is a monotone submodular set function.

Proof. Following the same strategy in Proposition 2, we can prove that $I(G_k; Z_j^\emptyset(\mathbf{A}))$ is a monotone submodular set function. Additionally, $V_2(\mathbf{A})$ is a positive linear combination of $I(G_k; Z_j^\emptyset(\mathbf{A}))$, thus $V_2(\mathbf{A})$ is a monotone submodular set function according to [55, pp.272]. \square

D. Planning for tracking and discovering objects using a multi-objective value function

To control a team of agents to track and discover, we consider the multi-objective value function

$$V(\mathbf{A}) = [V_1(\mathbf{A}), V_2(\mathbf{A})]^T, \quad (29)$$

where $\mathbf{A} \in \mathcal{M}$, while V_1 and V_2 are respectively described in (23) and (27). Multi-objective optimisation provides a meaningful notion of trade-off amongst objectives via the Pareto-set, wherein no solutions can improve one objective without degrading the other remaining ones [57]. Additionally, online planning requires choosing a solution from Pareto-set in a timely manner. One possible method is robust submodular observation selection (ROSS) [58] which selects a robust solution against the worst possible objective; however, the resulting value function is usually not submodular. Other alternative methods are the global criterion method (GCM) and weighted sum (WS), which are simple and retain the submodularity of the two value functions. Therefore, we choose GCM [59] to compute a trade-off solution by examining the distance of these two value functions from an ideal solution. The resulting value function from GCM is V_{mo} (with $V_{mo}(\emptyset) = 0$), given by:

$$V_{mo}(\mathbf{A}) = \sum_{i=1}^2 \frac{V_i(\mathbf{A}) - \min_{\mathbf{A} \in \mathcal{M}} V_i(\mathbf{A})}{\max_{\mathbf{A} \in \mathcal{M}} V_i(\mathbf{A}) - \min_{\mathbf{A} \in \mathcal{M}} V_i(\mathbf{A})}. \quad (30)$$

Algorithm 1 Greedy search algorithm

```

1: Input:  $\mathcal{M}$ ,  $V_{mo}$                                  $\triangleright$  action space and value function.
2: Output:  $\mathbf{A}_g \in \mathcal{M}$                        $\triangleright$  greedy control action.
3:  $\mathbf{A}_g := \emptyset$                                  $\triangleright$  initialise empty greedy control action.
4:  $P := \emptyset$                                      $\triangleright$  initialise empty planned agent's list.
5:  $U := \mathcal{N}$                                      $\triangleright$  initialise planning agent's list.
6: while  $U \neq \emptyset$  do
7:   for each  $n \in U$  do
8:      $[\mathbf{a}_g^{(n)}, V_c^{(n)}] := \arg \max_{\mathbf{a} \in \mathbf{A}^{(n)}} V_{mo}(\mathbf{A}_g \uplus \mathbf{a})$ 
9:   end for
10:   $n^* := \arg \max_{n \in U} V_c^{(n)}$             $\triangleright n^*$  that yields the best value function.
11:   $\mathbf{A}_g := \mathbf{A}_g \uplus \mathbf{a}_g^{(n^*)}$            $\triangleright$  store action with agent  $n^*$ .
12:   $P := P \cup \{n^*\}$                           $\triangleright$  add  $n^*$  into planned agent's list.
13:   $U := U \setminus \{n^*\}$                        $\triangleright$  delete  $n^*$  from planning agents' list.
14: end while

```

According to [60], GCM yields a unique solution. Thus, the multi-objective optimisation problem turns into

$$\mathbf{A}^* = \arg \max_{\mathbf{A} \in \mathcal{M}} V_{mo}(\mathbf{A}). \quad (31)$$

In principle, computing an optimal control action \mathbf{A}^* is a combinatorial optimisation problem, unless $V_{mo}(\mathbf{A})$ is a monotone submodular set function wherein a greedy algorithm can be implemented to reduce computational time significantly. To this end, we have the following result:

Corollary 5. V_{mo} in (30) is also a monotone submodular set function.

Proof. From Corollary 3 and Proposition 4, $V_1(\mathbf{A})$ and $V_2(\mathbf{A})$ are both monotone submodular set functions. Since $V_{mo}(\mathbf{A})$ is a positive linear combination of $V_1(\mathbf{A})$ and $V_2(\mathbf{A})$, thus $V_{mo}(\mathbf{A})$ is a monotone submodular set function, according to [55, pp.272]. \square

E. Greedy search algorithm

Let OPT denote the optimal value of a submodular function subject to a partition matroid \mathcal{M} , *i.e.*, $\text{OPT} = \max_{\mathbf{A} \in \mathcal{M}} V_{mo}(\mathbf{A})$. Since $V_{mo}(\cdot)$ is a monotone submodular set function (Corollary 5), it follows from [61] that a solution from a greedy search algorithm yields a lower bound performance at 0.5OPT (see Proposition 6, based on [61]).

Proposition 6. Let \mathbf{A}_g be the control action computed from a greedy search algorithm and $\text{OPT} = \max_{\mathbf{A} \in \mathcal{M}} V_{mo}(\mathbf{A})$. Then we have:

$$V_{mo}(\mathbf{A}_g) \geq 0.5\text{OPT}. \quad (32)$$

The above result justifies implementing a greedy search algorithm by including individual agents sequentially and selecting the next best agents that maximise the value function $V_{mo}(\cdot)$, as shown in Algorithm 1.

Remark 5. There are other alternatives such as the *randomised* algorithm which can achieve $(1 - 1/e)\text{OPT}$, see [62] and references therein for more details.



Fig. 3. CRAWDAD taxi dataset. There are 10 taxis travelling within an area of $6150 \text{ m} \times 6080 \text{ m}$ in San Francisco Bay Area over 1000 s. \bigcirc/\square symbols denote the Start/Stop positions of each taxi with different colours represent different taxis.

IV. EVALUATIONS OVER A REAL-WORLD DATASET

To demonstrate the performance of our proposed method, we conduct simulated experiments using the CRAWDAD taxi dataset [39] which contains several traces of taxis within the area of $6150 \text{ m} \times 6080 \text{ m}$ in San Francisco Bay Area, USA. In particular, we randomly selected 10 taxi tracks over 1000 s (from 18-May-2008 4:43:20 PM to 18-May-2008 5:00:00 PM), as shown in Fig. 3. Inspired by the approach in [27], the search area is scaled down by a factor of 5, while the time is sped up by the same factor of 5 so that the taxi's speed remains the same as in the real world. Thus, the simulated environment has an area of $1230 \text{ m} \times 1216 \text{ m}$ and a total search time of 200 s.

Since taxis can go into different routes, we employ the constant turn (CT) model with an unknown turn rate (see [63]) to account for its turning behaviour. In particular, let $\mathbf{x} = (x, \ell) \in \mathbb{T}$ denote the single object state comprising of label ℓ and kinematic state $x = [\tilde{x}^T, \theta]^T$ where $\tilde{x} = [\rho_x, \dot{\rho}_x, \rho_y, \dot{\rho}_y]^T$ is its position and velocity in Cartesian coordinates, and θ is the turn rate. Each object follows a constant turn model given by

$$\tilde{x}_{k+1|k} = F^{CT}(\theta_k) \tilde{x}_k + G^{CT} \eta_k, \quad (33)$$

$$\theta_{k+1|k} = \theta_k + T_0 q_k \quad (34)$$

where

$$F^{CT}(\theta) = \begin{bmatrix} 1 & \frac{\sin(\theta T_0)}{\theta} & 0 & -\frac{1 - \cos(\theta T_0)}{\theta} \\ 0 & \cos(\theta T_0) & 0 & -\sin(\theta T_0) \\ 0 & \frac{1 - \cos(\theta T_0)}{\theta} & 1 & \frac{\sin(\theta T_0)}{\theta} \\ 0 & \sin(\theta T_0) & 0 & \cos(\theta T_0) \end{bmatrix},$$

$$G^{CT} = \begin{bmatrix} \frac{T_0^2}{2} & 0 \\ T_0 & 0 \\ 0 & \frac{T_0^2}{2} \\ 0 & T_0 \end{bmatrix},$$

$T_0 = 1$ s is a sampling interval; $\eta_k \sim \mathcal{G}(0, \sigma_\eta^2 I_2)$ with $\sigma_\eta = 0.15$ m/s² and I_2 is the 2×2 identity matrix; $q_k \sim \mathcal{G}(0, \sigma_q^2)$, and $\sigma_q^2 = \pi/60$ rad/s. Here, $\mathcal{G}(\mu, \Sigma)$ denotes a Gaussian distribution with mean μ and covariance Σ .

The on-board sensor on each agent is range-limited subject to $r_{D,\max}$ and its detection probability follows:

$$P_D(\mathbf{x}, \mathbf{u}) = \begin{cases} P_D^{\max} & d(\mathbf{x}, \mathbf{u}) \leq r_D, \\ \max(0, P_D^{\max} - (d(\mathbf{x}, \mathbf{u}) - r_D)\hbar) & \text{otherwise,} \end{cases}$$

where $d(\mathbf{x}, \mathbf{u})$ is the distance between the object \mathbf{x} and agent \mathbf{u} . A noisy *position-based* sensor is considered in our experiments wherein a detected object x yields to a noisy position measurement z , given by: $z = [p_x, p_y]^T + v$. Here, $v \sim \mathcal{G}(0, R)$ with $R = \text{diag}(\sigma_x^2, \sigma_y^2)$. Notably, we selected parameters for our experiments based on the real-world experimental results in [64], [65]. In particular, the minimum altitude of UAVs is 126 m, and its maximum detection range is 218.2 m (corresponding to a top-down camera with an FoV of 120°). The on-board sensor is corrupted by false-alarm measurements with a clutter rate $\lambda = 0.0223$, and a maximum detection probability of $P_D^{\max} = 0.8825$ (see Table VIII in [65]). We see that the estimated position error for a UAV at 60 m altitude is 0.55 m for measurement noise [64]. Since our UAVs fly at higher altitude and the measurement noise is proportional to the UAV's altitude [66], we set our measurement noise $\sigma_x = \sigma_y = 0.55 \times 126/60 = 1.115$ m. Further, a total number of 10 UAVs (*e.g.*, quad-copters) are considered in this experiment, which departs at the centre of the search area, *i.e.*, $[615, 608, 126]^T$.

Since there is no prior knowledge about object's state, we model initial births at time $k = 0$ by a grid-based LMB density with parameters $\{(r_{B,0}^{(i)}, p_B^{(i)})\}_{i=1}^{N_B}$. Here, N_B is the number of birth parameters, $p_B^{(i)} = \mathcal{G}(x; m_B^{(i)}, \Sigma_B)$ with $\Sigma_B = \text{diag}([\Delta_x/2; 1; \Delta_y/2; 1])^2$ and $m_B^{(i)} = [\rho_{B,x}^{(i)}, 0, \rho_{B,y}^{(i)}, 0]^T$ where the position elements $\rho = (\rho_{B,x}, \rho_{B,y})$ are grid cells of the search area with (Δ_x, Δ_y) spacing in $x - y$ directions. For the next time step, we propose an adaptive birth procedure that incorporates the current grid occupancy information at time k into the birth probability at the next time $k+1$. Note that, since the number of occupancy grid cells N_\varkappa can be significantly large, which may impact the filtering time if there are too many birth parameters, we propose resizing the occupancy grid $\{(r_{\varkappa,+}^{(i)}, \varkappa_c^{(i)})\}_{i=1}^{N_\varkappa}$ to $\{(\bar{r}_\varkappa^{(i)}, m_B^{(i)})\}_{i=1}^{N_B}$, with $N_B \ll N_\varkappa$, using bicubic interpolation⁵ to efficiently improve the filtering time. The birth existence probability is then updated by:

$$\tilde{r}_\varkappa^{(i)} = 1 + \frac{\bar{r}_\varkappa^{(i)}}{\max(\bar{r}_\varkappa^{(i)})}; r_{B,+}^{(i)} = \frac{\tilde{r}_\varkappa^{(i)} (\sum_{i=1}^{N_B} r_{B,0}^{(i)})}{\sum_{i=1}^{N_B} \tilde{r}_\varkappa^{(i)}}, \quad (35)$$

to ensure the number of expected births (*i.e.*, $\sum_{i=1}^{N_B} r_{B,+}^{(i)}$) remains fixed over time.

For the *grid-based occupancy* estimator, we set a grid of 100×100 ($N_\gamma = 10,000$) with a cell size of 12.3 m \times 12.16 m. For *adaptive birth*, we use $r_{B,0}^{(i)} = 0.01 \forall i$, $N_B = 100$, $\Delta_x = 123$ m, $\Delta_y = 121.6$ m, *i.e.* $\rho \in \{0.5\Delta_x, 1.5\Delta_x, \dots, 9.5\Delta_x\} \times$

⁵In particular, we can use `imresize` — a common MATLAB command to resize images using bicubic interpolation.

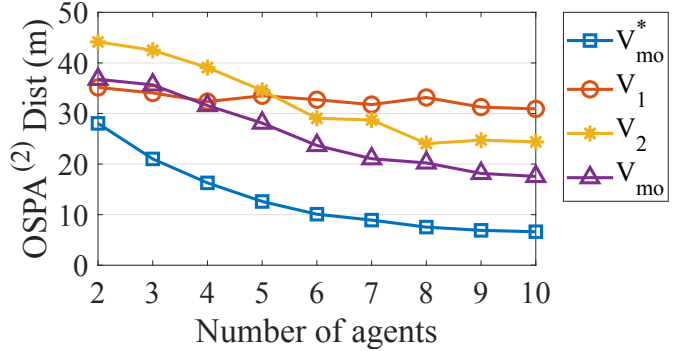


Fig. 4. CRAWDAD taxi dataset. Comparison between our multi-objective value function V_{mo} versus baseline methods over 20 Monte Carlo runs when $|\mathcal{N}|$ is increased from 2 to 10. V_{mo}^* is the best possible performance when the measurement origins are known (w/o data association).

$\{0.5\Delta_y, 1.5\Delta_y, \dots, 9.5\Delta_y\}$. The total search time is 200 s. All results are summarised over 20 Monte Carlo runs.

For tracking performance evaluation, we use the optimal sub-pattern assignment ($\text{OSPA}^{(2)}$) in [67] with cut-off $c = 50$ m, order $p = 1$, over a window length of 200-scan, *i.e.*, the entire experimental duration (see the Appendix B for how $\text{OSPA}^{(2)}$ is calculated). A smaller $\text{OSPA}^{(2)} \text{ Dist (m)}$ indicates a better tracking performance in terms of localisation, cardinality (number of objects), track fragmentation as well as track switching errors. Additionally, to provide deeper understanding and intuition, we also present (*i*) $\text{OSPA}^{(2)} \text{ Loc (m)}$ (a localisation component) and (*ii*) $\text{OSPA}^{(2)} \text{ Card (m)}$ (a cardinality component) to analyse the discovery performance).

A. Performance over an increasing number of agents

In this subsection, the experiments are conducted to validate the hypothesis that our proposed multi-objective value function V_{mo} outperforms a single objective that either focuses on tracking or discovering in terms of overall tracking performance. Therefore, we examine the performance of three following planning algorithms: (*i*) utilising a single *tracking* objective value function V_1 , (*ii*) utilising a single *discovering* objective value function V_2 , (*iii*) utilising a multi-objective value function V_{mo} that simultaneously optimises both tracking and discovering tasks. Additionally, we also analyse $V_{mo}(\cdot)$ versus the previous multi-objective value function $V_{mo}^*(\cdot)$ when the data association (measurement-to-object origin) is known [40], which can be considered as the best possible (upper bound) performance.

Fig. 4 shows tracking performance in terms of $\text{OSPA}^{(2)}$ **Dist** for tracking 10 taxis in CRAWDAD taxi dataset when the number of agents increases from 2 to 10. On the one hand, when the number of agents is small (less than four), we observe that our V_1 achieves a similar accuracy as our V_{mo} since there are not enough agents to cover the area, the team should focus on tracking objects instead of exploring. On the other hand, when the number of agents is large (more than four), our proposed multi-objective value function V_{mo} constantly outperforms V_1 and V_2 , since there are enough agents to perform both tracking and discovering tasks simultaneously. As expected, the tracking objective V_1 does not improve the

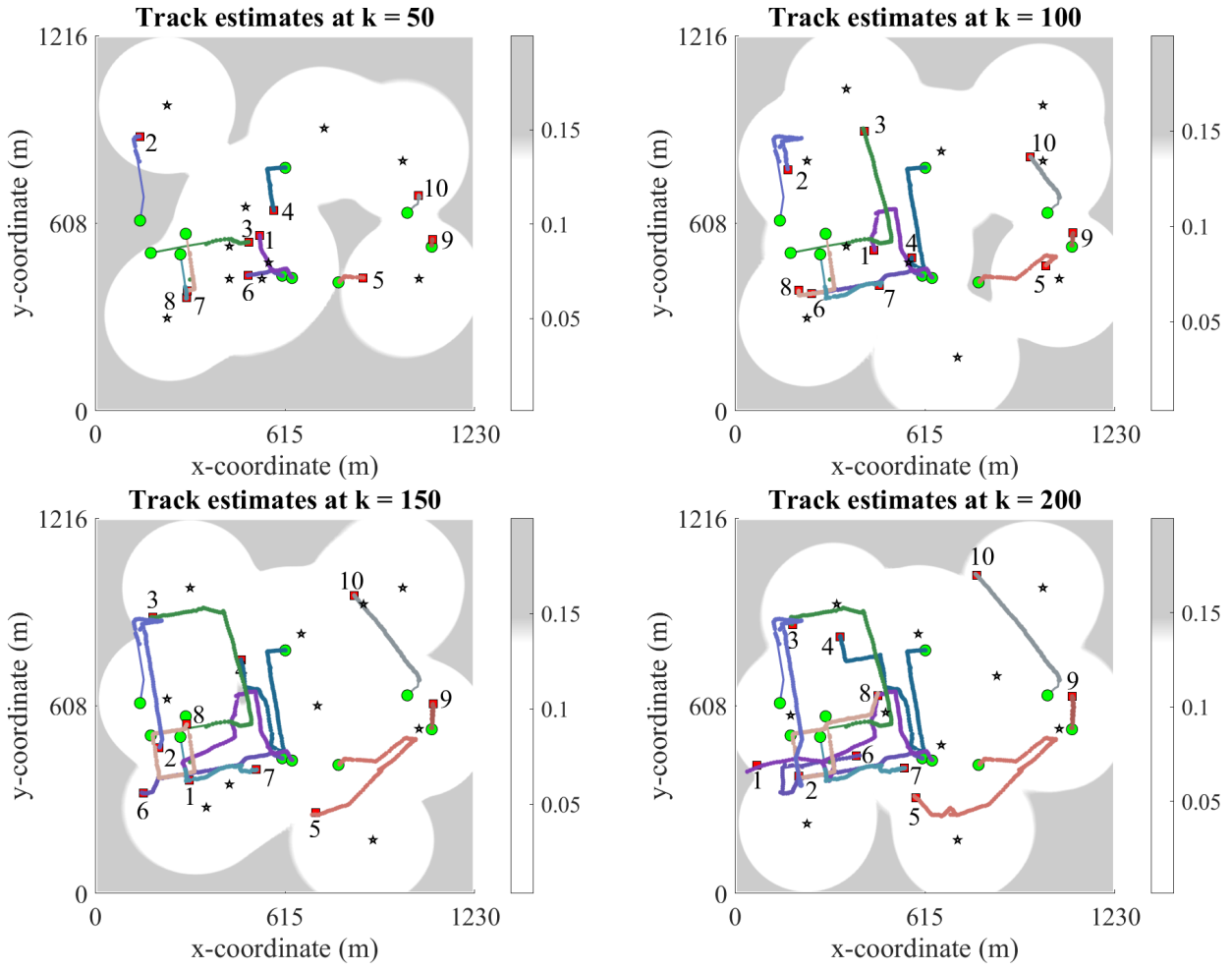


Fig. 5. CRAWDAD taxi dataset in a particular run using V_{mo} (jointly search and track objects). **Background:** the grid occupancy probability using 10 UAVs. **Foreground:** the estimated and true positions of 10 taxis. Solid lines represent the latest 50-step of UAV's trajectories, while dash lines represent the UAV's trajectories from start time at $k = 1$ to $k = 50$. Different colours represent different identities of the estimated objects. \bigcirc/\square symbols denote the Start/Stop positions of each object. The drone symbol denotes the UAV's positions.

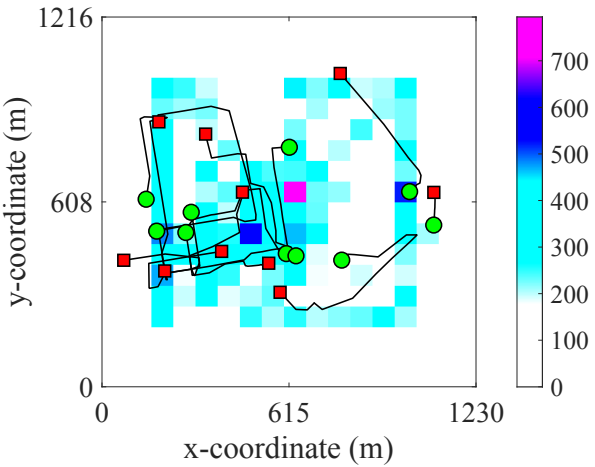


Fig. 6. CRAWDAD taxi dataset. The heatmap (16×16 grids) of trajectories for 10 UAVs over 20 MC runs using V_{mo} . \bigcirc/\square symbols denote the Start/Stop positions of each object. The colour bar represents the number of times the UAVs' positions inside a grid cell.

tracking performance when the number of agents increases since V_1 only focuses on tracking detected objects and is missing out detecting and tracking all of objects outside of their FoVs.

B. Detailed Experimental Results

In this subsection, we provide detailed experimental results to further demonstrate the effectiveness and insights of our proposed method when the number of UAVs is 10. Fig. 5 depicts the estimated trajectories versus the true trajectories of 10 taxi traces in the foreground, and the grid occupancy probability in the background, for the CRAWDAD tax dataset in a particular run using our proposed V_{mo} control method over time. The results demonstrate that we can correctly search and track all taxis with correct identities (different colours denote different taxis).

Fig. 6 further shows the the trajectory's heatmap for 10 UAVs over 20 MC runs. The outcome shows that our control method V_{mo} navigates 10 UAVs to concentrate more in the western region of the area of interest where there are more taxis around, while also slightly covering the eastern region to

successfully track the remaining taxis. It is expected that as time increases, the agents start to spread out from the centre to cover more area, which helps to detect and track more taxis. At the time $k = 100$ s, our agents can successfully detect all of 10 taxis. At the time $k = 165$ s, our method detects that two taxis disappear and stops tracking them. Consequently, we continue to track the 8 remaining taxis until they disappear from time 190 s to 200 s. Notably, even as the taxis randomly disappear over time, our method still effectively estimates the taxi positions, identities and the number of taxis, which demonstrates the robustness of our algorithm in the real-world dataset.

Fig. 7 details the overall mean and standard deviation ($\mu \pm 0.5\sigma$) to search and track 10 taxi traces for different control methods for 10 UAVs in terms of $\text{OSPA}^{(2)} \text{ Dist}$, $\text{OSPA}^{(2)} \text{ Loc}$, $\text{OSPA}^{(2)} \text{ Card}$ as well as the number of estimated taxis (*i.e.*, Cardinality) over 20 MC runs. The results show that our proposed V_{mo} consistently outperforms the tracking-only V_1 or discovering-only V_2 in terms of the overall tracking performance (*i.e.*, $\text{OSPA}^{(2)} \text{ Dist}$) over time. Further, for localisation error (*i.e.*, $\text{OSPA}^{(2)} \text{ Loc}$), the performance of V_{mo} approaches the performance of the ideal case V_{mo}^* . Additionally, we observe that most control methods can estimate the number of taxis (*i.e.*, Cardinality) correctly, except V_1 which only focuses on tracking and does not explore to find any taxis outside of the team's FoVs. In terms of $\text{OSPA}^{(2)} \text{ Card}$, which considers not only the cardinality estimates but also the track label switching and track fragmentation, we also observe that V_{mo} outperforms V_1 and V_2 . Notably, since the cardinality is estimated correctly, most $\text{OSPA}^{(2)} \text{ Card}$ errors come from the track label switching and track fragmentation errors, which is expected given the limited FoV sensors, and the motion model mismatch between the CT model and the taxi's occasional turns.

V. CONCLUSION

We have developed a multi-objective planning method for discovering and tracking multiple mobile objects for multi-agents with unknown data associations. The proposed multi-objective value function is shown to be monotone and submodular, thereby enabling low-cost implementation via greedy search. A series of comprehensive experiments on a real-world taxi dataset confirm our method's capability and efficiency. It also validates our proposed multi-objective method's robustness, wherein its overall performance shows decreasing trend over time similar to that of the best possible performance.

So far, we have considered a centralised MPOMDP for multi-agent planning where scalability can be a limitation. Moreover, the centralised approach can be a severe limitation of real-life cases when long-distance and a large number of agents (*e.g.*, UAVs) are required to explore a large area. A scalable approach should be a distributed POMDP for MOT, where each agent runs its local filter to track multiple objects and coordinates with other agents to achieve a global objective. However, planning for multiple agents to reach a global goal under a distributed POMDP framework is a NEXP-complete problem [22].

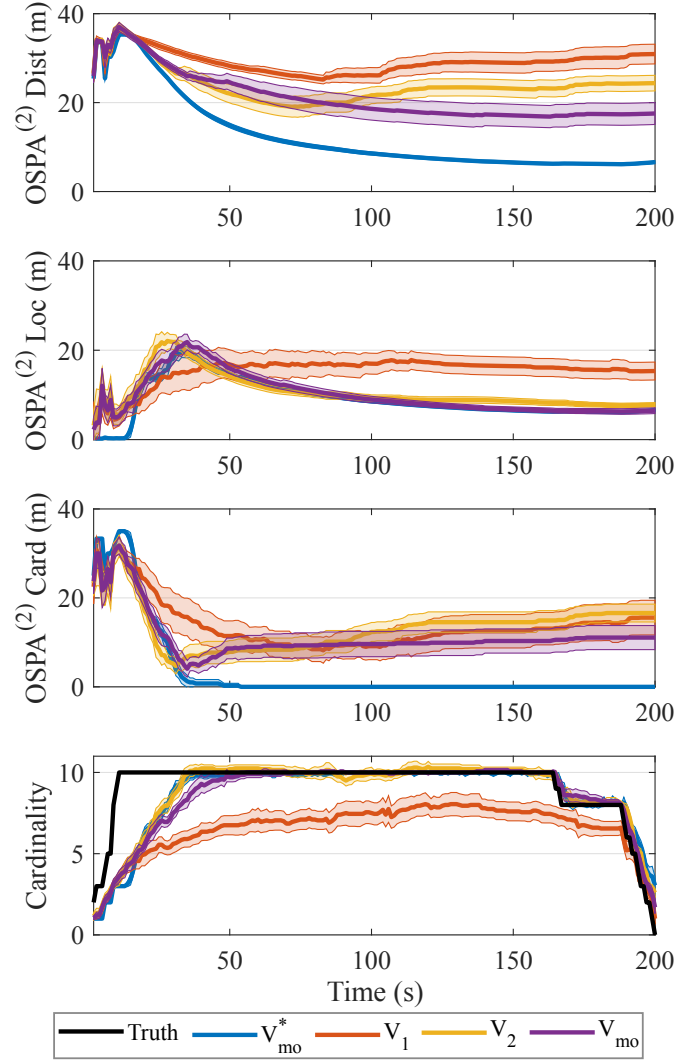


Fig. 7. CRAWDAD taxi dataset. The overall tracking performance ($\mu \pm 0.5\sigma$) over time over 20 MC runs using different control methods in terms of $\text{OSPA}^{(2)} \text{ Dist}$, $\text{OSPA}^{(2)} \text{ Loc}$, $\text{OSPA}^{(2)} \text{ Card}$, and the number of taxis (*i.e.*, Cardinality).

APPENDIX

A. MS-GLMB recursion

Under the standard multi-object system model the MS-GLMB recursion Ω taking the parameter-set

$$\pi \triangleq \left\{ \left(w^{(I, \xi)}, p^{(\xi)} \right) : (I, \xi) \in \mathcal{F}(\mathbb{L}) \times \Xi \right\}.$$

to the parameter-set

$$\pi_+ = \left\{ \left(w_+^{(I_+, \xi_+)}, p_+^{(\xi_+)} \right) : (I_+, \xi_+) \in \mathcal{F}(\mathbb{L}_+) \times \Xi_+ \right\}$$

is given by [38]

$$I_+ = \mathbb{B}_+ \uplus I, \quad \xi_+ = (\xi, \gamma_+) \quad (36)$$

$$w_+^{(I_+, \xi_+)} = 1_{\mathcal{F}(\mathbb{B}_+ \uplus I)}(\mathcal{L}(\gamma_+)) w^{(I, \xi)} \left[\omega^{(\xi, \gamma_+)} \right]^{\mathbb{B}_+ \uplus I} \quad (37)$$

$$p_+^{(\xi+)}(x_+, \ell) \propto \begin{cases} \langle \Lambda_S^{(\gamma+)}(x_+ | \cdot, \ell), p^{(\xi)}(\cdot, \ell) \rangle, & \ell \in \mathcal{L}(\gamma_+) - \mathbb{B}_+ \\ \Lambda_B^{(\gamma+)}(x_+, \ell), & \ell \in \mathcal{L}(\gamma_+) \cap \mathbb{B}_+ \end{cases} \quad (38)$$

$$\omega^{(\xi, \gamma+)}(\ell) = \begin{cases} 1 - \bar{P}_S^{(\xi)}(\ell), & \ell \in \overline{\mathcal{L}(\gamma_+)} - \mathbb{B}_+ \\ \bar{\Lambda}_S^{(\xi, \gamma+)}(\ell), & \ell \in \overline{\mathcal{L}(\gamma_+)} - \mathbb{B}_+, \\ 1 - P_{B,+}(\ell), & \ell \in \overline{\mathcal{L}(\gamma_+)} \cap \mathbb{B}_+, \\ \bar{\Lambda}_B^{(\gamma+)}(\ell), & \ell \in \mathcal{L}(\gamma_+) \cap \mathbb{B}_+ \end{cases} \quad (39)$$

$$\bar{P}_S^{(\xi)}(\ell) = \langle P_S(\cdot, \ell), p^{(\xi)}(\cdot, \ell) \rangle, \quad (40)$$

$$\Lambda_B^{(\gamma+)}(x_+, \ell) = \psi^{(\gamma+)}(x_+, \ell) f_{B,+}(x_+, \ell) P_{B,+}(\ell), \quad (41)$$

$$\Lambda_S^{(\gamma+)}(x_+ | y, \ell) = \psi^{(\gamma+)}(x_+, \ell) f_{S,+}(x_+ | y, \ell) P_S(y, \ell), \quad (42)$$

$$\bar{\Lambda}_B^{(\gamma+)}(\ell) = \int \Lambda_B^{(\gamma+)}(x, \ell) dx, \quad (43)$$

$$\bar{\Lambda}_S^{(\xi, \gamma+)}(\ell) = \int \langle \Lambda_S^{(\gamma+)}(x | \cdot, \ell), p^{(\xi)}(\cdot, \ell) \rangle dx. \quad (44)$$

$$\psi^{(\gamma)}(\mathbf{x}) \triangleq \prod_{n \in \mathcal{N}} \psi^{(n, \gamma^{(n)})}(\mathbf{x}). \quad (45)$$

$$\psi^{(n, \gamma^{(n)})}(\mathbf{x}) = \begin{cases} 1 - P_D^{(n)}(\mathbf{x}), & \gamma^{(n)}(\mathcal{L}(\mathbf{x})) = 0 \\ \frac{P_D^{(n)}(\mathbf{x}) g^{(n)}(z_j^{(n)} | \mathbf{x})}{\kappa^{(a)}(z_j^{(n)})}, & \gamma^{(n)}(\mathcal{L}(\mathbf{x})) = j > 0 \end{cases} \quad (46)$$

B. Performance evaluation metric

Optimal Sub-Pattern Assignment (OSPA) metric: The traditional performance metric using root mean square error (RMSE) is not applicable to evaluate our considered scenarios wherein the number of objects is time-varying. The reason is that RMSE does not have a clear concept of error for the cases when the number of estimated objects is not equal to the number of ground truths. As a result, [68] has proposed a mathematically and intuitively consistent metric—OSPA—to address the aforementioned miss-distance concept.

Let $d_0^{(p,c)}(X, Y)$ be the OSPA distance (so-called **OSPA Dist**) between $X, Y \in \mathcal{F}(\mathbb{X})$ with order $p \geq 1$ and cut-off $c > 0$ with $X = \{x^{(1)}, \dots, x^{(m)}\}$ and $Y = \{y^{(1)}, \dots, y^{(n)}\}$. If $m \leq n$, $d_0^{(p,c)}(X, Y)$ is defined as:

$$d_0^{(p,c)}(X, Y) = \left(\frac{1}{n} \left(\min_{\pi \in \Pi_n} \sum_{i=1}^m \bar{d}^{(c)}(x^{(i)}, y^{(\pi(i))})^p + c^p(n-m) \right) \right)^{1/p}, \quad (47)$$

where Π_n is a set of all permutations of n ($|\Pi_n| = n!$), $\bar{d}^{(c)}(x, y) = \min(c, d(x, y))$ is a base distance, in which $d(\cdot, \cdot)$ is an arbitrary metric on the single object state space of \mathbb{X} (e.g., Euclidean distance). If $m > n$, then $d_0^{(p,c)}(X, Y) \triangleq d_0^{(p,c)}(Y, X)$.

The **OSPA Dist** has two components: *OSPA Loc* $d_{0,loc}^{(p,c)}$ and *OSPA Card* $d_{0,card}^{(p,c)}$ to account for localisation and cardinality errors, respectively. These components are computed as:

$$d_{0,loc}^{(p,c)}(X, Y) = \left(\frac{1}{n} \min_{\pi \in \Pi_n} \sum_{i=1}^m \bar{d}^{(c)}(x^{(i)}, y^{(\pi(i))})^p \right)^{1/p}, \quad (48)$$

$$d_{0,card}^{(p,c)}(X, Y) = \left(\frac{c^p(n-m)}{n} \right)^{1/p}, \quad (49)$$

where $m \leq n$. If $m > n$, then $d_{0,loc}^{(p,c)}(X, Y) \triangleq d_{0,loc}^{(p,c)}(Y, X)$, $d_{0,card}^{(p,c)}(X, Y) \triangleq d_{0,card}^{(p,c)}(Y, X)$.

Since we consider multi-object tracking, which focuses not only the objects' positions but also their trajectories over time [43], we need a metric to evaluate the tracking performance meaningfully. In this work, we use the $\text{OSPA}^{(2)}$ metric [67] to measure the dissimilarity between two sets of tracks. The $\text{OSPA}^{(2)}$ metric is the OSPA metric with its *base distance* is itself another OSPA-based metric. In particular, $\text{OSPA}^{(2)}$ takes into consideration for the occurrences of track switching and track fragmentation.

Base distance: Let $\mathbb{D} = \{1, \dots, \mathcal{D}\}$ be the finite space of time indices, from the start time at 1 to the end time at \mathcal{D} . Let $\mathbb{C} \triangleq \{f : \mathbb{D} \rightarrow \mathbb{X}\}$ be the space of all functions from \mathbb{D} to \mathbb{X} . A track is an element of \mathbb{C} . Let $f, g \in \mathbb{C}$ be two tracks, with time supports $D_f, D_g \in \mathbb{D}$, respectively. The base distance between two tracks is defined as the average OSPA distance over its time support, *i.e.*,

$$\tilde{d}^{(c)}(f, g) = \sum_{t \in D_f \cup D_g} \frac{d_0^{(c)}(\{f(t)\}, \{g(t)\})}{|D_f \cup D_g|}, \quad (50)$$

if $|D_f \cup D_g| \neq 0$, and 0 if otherwise. Here, $\{f(t)\}$ is a singleton if $t \in D_f$, and empty set otherwise (same for $\{g(t)\}$), and $d_0^{(c)}(\cdot, \cdot)$ is the OSPA distance defined in (47) where parameter p no longer becomes operative since the input arguments have at most one element, which becomes

$$d_0^{(c)}(\{f(t)\}, \{g(t)\}) = \begin{cases} 0, & \text{if } |\{f(t)\}| = |\{g(t)\}| = 0, \\ c, & \text{if } |\{f(t)\}| \neq |\{g(t)\}|, \\ \min(c, d(f(t), g(t))), & \text{if } |\{f(t)\}| = |\{g(t)\}| = 1. \end{cases} \quad (51)$$

OSPA⁽²⁾ metric for tracks: According to [67], the base distance $\tilde{d}^{(c)}(\cdot, \cdot)$ in (50) has a maximum value of c and is also a metric. As a result, we can use this base distance in the original OSPA metric. Suppose $X = \{f^{(1)}, \dots, f^{(m)}\} \in \mathcal{F}(\mathbb{C})$ and $Y = \{g^{(1)}, \dots, g^{(n)}\} \in \mathcal{F}(\mathbb{C})$ are two sets of tracks, the OSPA⁽²⁾ distance (so-called **OSPA⁽²⁾ Dist**) $\check{d}_p^{(c)}(X, Y)$, with c is the cut-off and p is the order parameters, is defined as:

$$\check{d}_p^{(c)}(X, Y) = \left(\frac{1}{n} \left(\min_{\pi \in \Pi_n} \sum_{i=1}^m \tilde{d}^{(c)}(f^{(i)}, g^{(\pi(i))})^p + c^p(n-m) \right) \right)^{1/p}, \quad (52)$$

where $m < n$. If $m > n$, then $\check{d}_p^{(c)}(X, Y) \triangleq \check{d}_p^{(c)}(Y, X)$. The OSPA⁽²⁾ is proved to be a metric, and provides physically meaningful distance between two sets of tracks that takes

into account localisation, cardinality, track identity and track fragmentation errors.

Similarly to the **OSPA Dist**, the **OSPA⁽²⁾ Dist** also has two components: *i*) **OSPA⁽²⁾ Loc** $\check{d}_{0,loc}^{(p,c)}$ to account for localisation error and *ii*) **OSPA⁽²⁾ Card** $\check{d}_{0,card}^{(p,c)}$ to account for cardinality, track identity and track fragmentation errors. These components are computed as:

$$\check{d}_{0,loc}^{(p,c)}(X, Y) = \left(\frac{1}{n} \min_{\pi \in \Pi_n} \sum_{i=1}^m \check{d}^{(c)}(f^{(i)}, g^{(\pi(i))})^p \right)^{1/p}, \quad (53)$$

$$\check{d}_{0,card}^{(p,c)}(X, Y) = \left(\frac{c^p(n-m)}{n} \right)^{1/p}, \quad (54)$$

where $m \leq n$. If $m > n$, then $\check{d}_{0,loc}^{(p,c)}(X, Y) \triangleq \check{d}_{0,loc}^{(p,c)}(Y, X)$, $\check{d}_{0,card}^{(p,c)}(X, Y) \triangleq \check{d}_{0,card}^{(p,c)}(Y, X)$.

C. Mathematical proofs

Proof of Proposition 1

Substituting (LMB density) for $\pi(\mathbf{X})$, using the abbreviation $W = -\sum_{L \subseteq \mathbb{L}} w(L) \log(w(L))$, we have:

$$\begin{aligned} h(\mathbf{X}) &= - \int \pi(\mathbf{X}) \log(K^{|\mathbf{X}|} \pi(\mathbf{X})) \delta \mathbf{X} \\ &= - \int w(\mathcal{L}(\mathbf{X})) p^{\mathbf{X}} \log w(\mathcal{L}(\mathbf{X})) \delta \mathbf{X} \\ &\quad - \int w(\mathcal{L}(\mathbf{X})) p^{\mathbf{X}} \log(K^{|\mathbf{X}|} p^{\mathbf{X}}) \delta \mathbf{X} \\ &= -W - \sum_{n=1}^{\infty} \frac{1}{n!} \sum_{(\ell_1, \dots, \ell_n) \in \mathbb{L}^n} \delta_n(|\{\ell_1, \dots, \ell_n\}|) w(\{\ell_1, \dots, \ell_n\}) \\ &\quad \times \int \prod_{j=1}^n p^{(\ell_j)}(x_j) \log \left(K^n \prod_{i=1}^n p^{(\ell_i)}(x_i) \right) dx_1 \dots dx_n \end{aligned} \quad (55)$$

where $\int w(\mathcal{L}(\mathbf{X})) \log w(\mathcal{L}(\mathbf{X})) p^{\mathbf{X}} \delta \mathbf{X} = W$ follows from Lemma 3 of [43]. Now, consider:

$$\begin{aligned} &\int \prod_{j=1}^n p^{(\ell_j)}(x_j) \log \left(\prod_{i=1}^n [K p^{(\ell_i)}(x_i)] \right) dx_1 \dots dx_n \\ &= \int \prod_{j=1}^n p^{(\ell_j)}(x_j) \sum_{i=1}^n \left(\log [K p^{(\ell_i)}(x_i)] \right) dx_1 \dots dx_n \\ &= \sum_{i=1}^n \left(\int p^{(\ell_i)}(x_i) \log [K p^{(\ell_i)}(x_i)] dx_i \times \right. \\ &\quad \left. \prod_{j \in \{1, \dots, n\} \setminus \{i\}} \int p^{(\ell_j)}(x_j) dx_j \right) \\ &= \sum_{i=1}^n \int p^{(\ell_i)}(x) \log [K p^{(\ell_i)}(x)] dx \end{aligned} \quad (56)$$

Substituting (56) into (55), we have:

$$\begin{aligned} h(\mathbf{X}) &= - \sum_{L \subseteq \mathbb{L}} w(L) \log(w(L)) \\ &\quad - \sum_{\substack{L \subseteq \mathbb{L} \\ L \neq \emptyset}} w(L) \left(\sum_{\ell \in L} \int p^{(\ell)}(x) \log [K p^{(\ell)}(x)] dx \right). \square \end{aligned}$$

Proof of Proposition 2: We want to prove that this mutual information $q_I(\mathbf{A}) \triangleq I(\mathbf{X}; \mathbf{Z}(\mathbf{A}))$ is a monotone submodular set function, that is $\forall \mathbf{A} \subseteq \mathbf{B} \subset \mathbf{A}$ and $\forall \mathbf{a} \in \mathbf{A} \setminus \mathbf{B}$:

$$q(\mathbf{B} \cup \{\mathbf{a}\}) - q(\mathbf{B}) \leq q(\mathbf{A} \cup \{\mathbf{a}\}) - q(\mathbf{A}), \quad (57)$$

$$\begin{aligned} &\Leftrightarrow I(\mathbf{X}; \mathbf{Z}(\mathbf{B} \cup \{\mathbf{a}\})) - I(\mathbf{X}; \mathbf{Z}(\mathbf{B})) \\ &\leq I(\mathbf{X}; \mathbf{Z}(\mathbf{A} \cup \{\mathbf{a}\})) - I(\mathbf{X}; \mathbf{Z}(\mathbf{A})). \end{aligned} \quad (58)$$

According to (3.53) and (25.36) in [15], we have: $\int \pi_Z(\mathbf{Z}_1 \cup \mathbf{Z}_2) \delta(\mathbf{Z}_1 \cup \mathbf{Z}_2) = \int \pi_Z(\mathbf{Z}_1, \mathbf{Z}_2) \delta \mathbf{Z}_1 \delta \mathbf{Z}_2$. Thus, (58) is equivalent to

$$\begin{aligned} &I(\mathbf{X}; \mathbf{Z}(\mathbf{B}), \mathbf{Z}(\mathbf{a}))) - I(\mathbf{X}; \mathbf{Z}(\mathbf{B})) \\ &\leq I(\mathbf{X}; \mathbf{Z}(\mathbf{A}), \mathbf{Z}(\mathbf{a})) - I(\mathbf{X}; \mathbf{Z}(\mathbf{A})). \end{aligned} \quad (59)$$

Based on the definition (see (14)), *i.e.*, $\mathbf{Z}(\mathbf{A}) = \uplus_{\alpha \in \mathbf{A}} \mathbf{Z}(\alpha)$, and because $\mathbf{A} \subseteq \mathbf{B}$, $\mathbf{a} \in \mathbf{A} \setminus \mathbf{B}$, we have: $\mathbf{Z}(\mathbf{A}) \subseteq \mathbf{Z}(\mathbf{B})$ and $\mathbf{Z}(\mathbf{a}) \in \mathbf{Z} \setminus \mathbf{Z}(\mathbf{B})$.

Thus, proving (59) is equivalent to proving $\forall \mathbf{R} \subseteq \mathbf{Z} \subseteq \mathbf{Z}$ and $\forall \mathbf{z} \in \mathbf{Z} \setminus \mathbf{Z}$:

$$I(\mathbf{X}; \mathbf{Z}, \mathbf{z}) - I(\mathbf{X}; \mathbf{Z}) \leq I(\mathbf{X}; \mathbf{R}, \mathbf{z}) - I(\mathbf{X}; \mathbf{R}). \quad (60)$$

Since $\mathbf{R} \subseteq \mathbf{Z} \subseteq \mathbf{Z}$, using mutual information inequalities [50, p.50], we have:

$$I(\mathbf{Z}; \mathbf{z}) \geq I(\mathbf{R}; \mathbf{z}), \quad (61)$$

$$\Leftrightarrow h(\mathbf{z}) - h(\mathbf{z}|\mathbf{Z}) \geq h(\mathbf{z}) - h(\mathbf{z}|\mathbf{R}), \quad (62)$$

$$\Leftrightarrow h(\mathbf{z}|\mathbf{R}) \geq h(\mathbf{z}|\mathbf{Z}), \quad (63)$$

$$\Leftrightarrow h(\mathbf{R}, \mathbf{z}) - h(\mathbf{R}) \geq h(\mathbf{Z}, \mathbf{z}) - h(\mathbf{Z}). \quad (64)$$

Further, $I(\mathbf{Z}; \mathbf{z}|\mathbf{X}) = I(\mathbf{R}; \mathbf{z}|\mathbf{X}) = 0$ is due to \mathbf{z} is independent of \mathbf{R} and \mathbf{Z} given \mathbf{X} , we have:

$$\begin{aligned} h(\mathbf{z}|\mathbf{X}) &= h(\mathbf{z}|\mathbf{X}, \mathbf{Z}) + I(\mathbf{Z}; \mathbf{z}|\mathbf{X}) = h(\mathbf{z}|\mathbf{X}, \mathbf{Z}) \\ &= h(\mathbf{X}, \mathbf{Z}, \mathbf{z}) - h(\mathbf{X}, \mathbf{Z}), \end{aligned} \quad (65)$$

$$\begin{aligned} h(\mathbf{z}|\mathbf{X}) &= h(\mathbf{z}|\mathbf{X}, \mathbf{R}) + I(\mathbf{R}; \mathbf{z}|\mathbf{X}) \\ &= h(\mathbf{X}, \mathbf{R}, \mathbf{z}) - h(\mathbf{X}, \mathbf{R}). \end{aligned} \quad (66)$$

Hence

$$h(\mathbf{X}, \mathbf{Z}, \mathbf{z}) - h(\mathbf{X}, \mathbf{Z}) = h(\mathbf{X}, \mathbf{R}, \mathbf{z}) - h(\mathbf{X}, \mathbf{R}). \quad (67)$$

Subtracting (64) from (67), we have:

$$\begin{aligned} &[h(\mathbf{X}, \mathbf{Z}, \mathbf{z}) - h(\mathbf{X}, \mathbf{Z})] - [h(\mathbf{Z}, \mathbf{z}) - h(\mathbf{Z})] \\ &\geq [h(\mathbf{X}, \mathbf{R}, \mathbf{z}) - h(\mathbf{X}, \mathbf{R})] - [h(\mathbf{R}, \mathbf{z}) - h(\mathbf{R})] \end{aligned} \quad (68)$$

Using differential entropy chain rules [50, p.253], we have that $h(\mathbf{X}|\mathbf{Z}, \mathbf{z}) = h(\mathbf{X}, \mathbf{Z}, \mathbf{z}) - h(\mathbf{Z}, \mathbf{z})$ and $h(\mathbf{X}|\mathbf{Z}) = h(\mathbf{X}, \mathbf{Z}) - h(\mathbf{Z})$, thus the above equation is equivalent to

$$h(\mathbf{X}|\mathbf{Z}, \mathbf{z}) - h(\mathbf{X}|\mathbf{Z}) \geq h(\mathbf{X}|\mathbf{R}, \mathbf{z}) - h(\mathbf{X}|\mathbf{R}) \quad (69)$$

$$\begin{aligned} &\Leftrightarrow [h(\mathbf{X}) - h(\mathbf{X}|\mathbf{Z}, \mathbf{z})] - [h(\mathbf{X}) - h(\mathbf{X}|\mathbf{Z})] \\ &\leq [h(\mathbf{X}) - h(\mathbf{X}|\mathbf{R}, \mathbf{z})] - [h(\mathbf{X}) - h(\mathbf{X}|\mathbf{R})], \end{aligned} \quad (70)$$

$$\Leftrightarrow I(\mathbf{X}; \mathbf{Z}, \mathbf{z}) - I(\mathbf{X}; \mathbf{Z}) \leq I(\mathbf{X}; \mathbf{R}, \mathbf{z}) - I(\mathbf{X}; \mathbf{R}). \quad (71)$$

Thus, $I(\mathbf{X}; \mathbf{Z}(\mathbf{A}))$ is a *submodular* set function. Further, using the chain rule we have:

$$\begin{aligned} &I(\mathbf{X}; \mathbf{Z}(\mathbf{A}), \mathbf{Z}(\mathbf{a})) - I(\mathbf{X}; \mathbf{Z}(\mathbf{A})) \\ &= I(\mathbf{X}; \mathbf{Z}(\mathbf{A})|\mathbf{Z}(\mathbf{a})) \geq 0 \end{aligned} \quad (72)$$

Hence, $I(\mathbf{X}; \mathbf{Z}(\mathbf{A}))$ is a *monotone submodular* set function of \mathbf{A} \square .

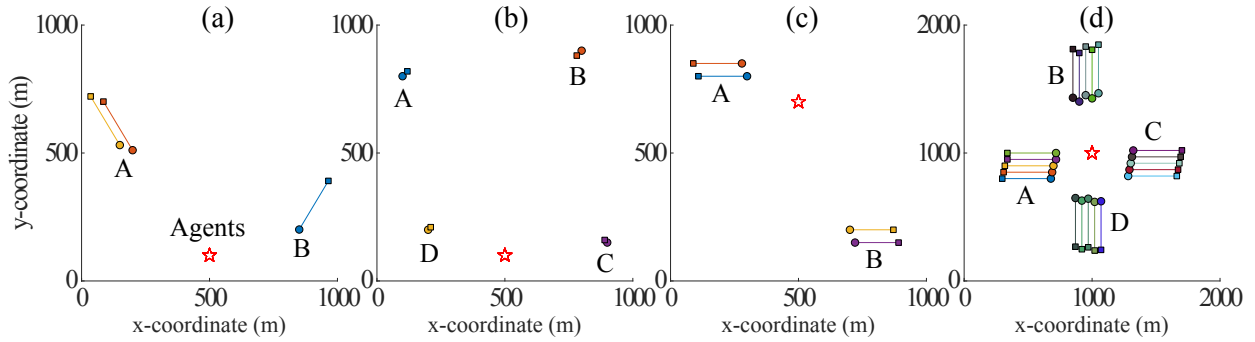


Fig. 8. Experimental settings for four scenarios (a) Scenario 1; (b) Scenario 2; (c) Scenario 3; (d) Scenario 4. The red \star symbol denotes the agents' initial positions. \bigcirc/\square symbols denote the Start/Stop positions of each object.

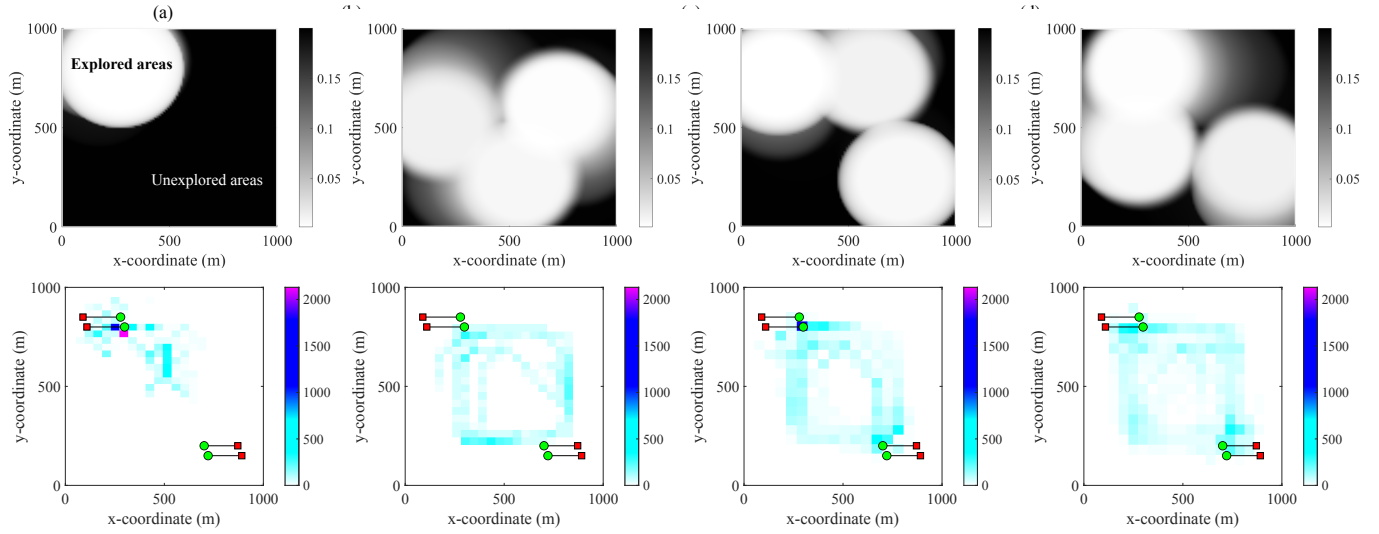


Fig. 9. Scenario 3 (Opposite) - grid occupancy probability at final time $k = 200$ s (top) and heatmap of trajectories (bottom) for 3 agents over 20 MC runs with $r_D = 200$ m using (a) V_1 : late-birth group B never discovered, (b) V_2 : extensive exploration, (c) V_{mo} : discovers the late birth group B while tracking both groups, and (d) V_{mo}^* : upper performance bound when the measurement origins are known.

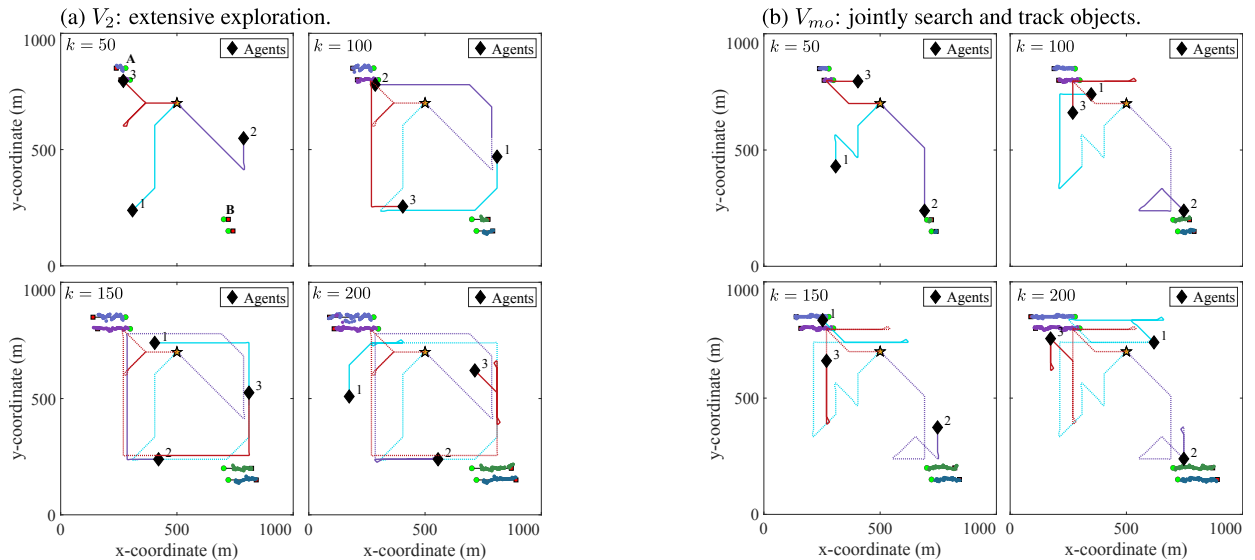


Fig. 10. Scenario 3 (Opposite) — The trajectories of three agents as well as the estimated and true positions of objects in a particular run using (a) V_2 (extensive exploration) making all three agents moving in an anti-clockwise circle to discover objects, (b) V_{mo} (jointly search and track objects) making agent 2 discovered and subsequently tracked the far-away objects of group B in the south-east region while agent 1 and agent 3 switch roles of exploring and tracking the nearby objects of group A in the north-west region. Solid lines represent the latest 50-step of agent's trajectories, while dash lines represent the agent's trajectories from start time at $k = 1$ to $k = 50$. Different colours represent different identities (labels) of agents and estimated objects.

D. Numerical Experiments

In this section, the proposed multi-objective value function is comprehensively evaluated using various synthetic experiments to control all of the system's parameters, especially for planning to track a time-varying number of objects. We consider four different scenarios to further demonstrate the robustness of our system, as depicted in Fig. 8.

Scenario 1 (FastMoving) — *fast-moving objects* (Fig. 8a): two groups of three fast mobile objects that move in a similar direction.

Scenario 2 (LateBirth) — *late-birth objects* (Fig. 8b): four slow objects with two groups, C and D , enter the scene late at time $k = 100$. This is the most challenging setup that favours the discovering value function V_2 to detect late-birth objects.

Scenario 3 (Opposite) — *two groups of four objects scurries in opposing directions* (Fig. 8c): The chance of detecting group B , which is out of the sensor's detection range, can only be realised through exploration.

Scenario 4 (Explosion) — *objects move in opposing directions* (Fig. 8d): Four groups of 20 fast-moving objects that run in four opposing directions.

The following provides detailed experimental settings.

Experimental settings: We study a team of quad-copter drones is conducting surveillance tasks in four different scenarios, wherein the area of the first three cases are $1000 \text{ m} \times 1000 \text{ m}$, while the area in scenario 4 is $2000 \text{ m} \times 2000 \text{ m}$. We control agents to fly and maintain at a different altitude to avoid collisions with the minimum altitude is 30 m , and the altitude gap amongst agents is 5 m . For computational simplicity, we consider two-dimensional (2D) tracking by assuming that all objects stay on a horizontal plane. Let $\mathbf{x} = (x, \ell) \in \mathbb{T}$ denote the single object state comprising of label ℓ and kinematic state $x = [\rho_x, \dot{\rho}_x, \rho_y, \dot{\rho}_y]^T$ in Cartesian coordinates. Each object follows a constant velocity model given by $x_{k+1|k} = F^{CV} x_k + q_k^{CV}$. Here, $F^{CV} = [1, T_0; 0, T_0] \otimes I_2$ with $T_0 = 1 \text{ s}$ is a sampling interval; \otimes denotes for the Kronecker product; I_2 is the 2×2 identity matrix; $q_k^{CV} \sim \mathcal{N}(0, \Sigma^{CV})$ is a 4×1 zero mean Gaussian process noise, with co-variance $\Sigma^{CV} = \sigma_{CV}^2 [T_0^3/3, T_0^2/2; T_0^2/2, T_0] \otimes I_2$.

The on-board sensor on each agent n is range-limited subject to $r_{D,\max} = 200 \text{ m}$ and its detection probability follows: where $P_D^{\max} = 0.8$, $\hbar = 0.008 \text{ m}^{-1}$. The on-board sensor measurement is also corrupted by false-alarm measurements which follows a Poisson RFS with a clutter rate $\lambda = 25$. A noisy *position-based* sensor is considered in our experiments wherein a detected object x yields to a noisy position measurement z , given by: $z = [p_x, p_y]^T + v$. Here, $v \sim \mathcal{N}(0, R)$ with $R = \text{diag}(\sigma_x^2, \sigma_y^2)$ where $\sigma_x = \sigma_y = \sigma_{0,xy} + \beta_{xy} \|x_p - u^{(n)}\|$ with $\sigma_{0,xy} = 10 \text{ m}$, and $\beta_{xy} = 0.01$.

For the *grid-based occupancy* estimator, we set a grid of 100×100 ($N_\gamma = 10,000$) across four scenarios, *i.e.*, scenario 1,2 and 3 have a cell size of $10 \text{ m} \times 10 \text{ m}$, scenario 4 has a cell size of $20 \text{ m} \times 20 \text{ m}$. For *adaptive birth*, we use $r_{B,0}^{(i)} = 0.01 \forall i$, $N_B = 100$, $\Delta_x = \Delta_y = 100 \text{ m}$ for Scenario 1,2, and 3 while $\Delta_x = \Delta_y = 200 \text{ m}$ for scenario 4. The total search time is 200 s . All reported results are summarised over 20 Monte Carlo runs.

Results. The detailed performance comparison for all four scenarios over 20 Monte Carlo runs is provided in Table I. The results confirm that our hypothesis of *the proposed multi-objective value function V_{mo} consistently outperforms other value functions in terms of $OSPA^{(2)} \text{ Dist}$ (the overall performance)* is correct. The reason is that V_{mo} simultaneously focuses on tracking detected objects while discovering undetected ones. It also affirms the effectiveness of our multi-object value function V_{mo} , which approaches the best possible performance of V_{mo}^* . For further insight, the results also validate our intuition that V_1 performs best in terms of $OSPA^{(2)} \text{ Loc}$ since it only focuses on tracking, and V_2 has the best results in $OSPA^{(2)} \text{ Card}$ and the smallest *Entropy*⁶ since it only focuses on discovering.

Fig. 9 depicts the grid occupancy and the trajectory's heatmap of 3-agents in scenario 3, and Fig. 10 shows detailed trajectories of three agents, and estimated and true positions of objects over different time steps in a particular run for scenario 3. On the one hand, V_1 never discovers group B in the southeast region since it only focuses on tracking the already discovered objects of group A in the northwest region, as shown in Fig. 9a. On the other hand, V_2 can easily discover all objects, regardless of their positions, since V_2 focuses on the discovering task, which renders the three agents circling the survey area in a counter-clockwise direction through times, as shown in Fig. 9b and Fig. 10a. However, since V_2 does not focus on tracking, V_2 yields a mediocre localisation accuracy, *i.e.*, estimated positions of objects significantly fluctuate around their true locations (see Fig. 10a). In contrast, by combining the strengths of V_1 and V_2 , V_{mo} not only discovers all objects but also tracks them well, as depicted in Fig. 9c and Fig. 10b. In particular, from $k = 1$ to $k = 50$, sensor 3 detects objects in group A, thus sensor 3 moves to the northwest region to track them while sensor 1 and sensor 2 are conducting the exploring task. From time $k = 50$ to $k = 100$, sensor 2 detects objects in group B; hence, it moves around the southeast region to track them (likewise for sensor 3 to stay at the northwest region to track objects in group A). On the other hand, sensor 1 continues to do exploring in the southwest region and moves to the northwest region to support sensor 1 for tracking objects. From $k = 100$ to $k = 150$, sensor 2 continues to stay at the southeast region to track objects in group B. In contrast, sensor 1 switches roles with sensor 3, *i.e.*, sensor 1 focuses on tracking objects in group and sensor 3 focuses on exploring the west area. A similar behaviour observed from $k = 150$ to $k = 200$ such that sensor 2 maintains in the southeast region to accurately track objects in group B. In contrast, sensor 1 and sensor 3 switch roles again, *i.e.*, sensor 1 focuses on exploring the area in the northeast corner and sensor 3 focuses on tracking objects in group A. Therefore, the results validate the efficiency of our proposed multi-objective value function wherein agents not only focus on track but also on discovering out-of-range fast-moving objects.

⁶*Entropy (nats)* is an averaged grid occupancy entropy to analyse the team's coverage region.

TABLE I

AVERAGED TRACKING PERFORMANCE OVER THE ENTIRE EXPERIMENTAL DURATION OF 20 MONTE CARLO RUNS AMONGST FOUR DIFFERENT VALUE FUNCTIONS ACROSS FOUR SCENARIOS WITH DETECTION RANGE $r_D = 200$ M. V_{mo} IS OUR PROPOSED MULTI-OBJECTIVE VALUE FUNCTION, WHILE V_{mo}^* IS THE BEST POSSIBLE PERFORMANCE WHEN THE MEASUREMENT ORIGINS ARE KNOWN (W/O DATA ASSOCIATION).

		Scenario 1 (FastMoving)				Scenario 2 (LateBirth)				
Agents	Indicators	<i>Overall performance</i>	Tracking performance	Discovery performance		<i>Overall performance</i>	Tracking performance	Discovery performance		
		OSPA⁽²⁾	OSPA⁽²⁾	<i>Loc (m)</i>	<i>OSPA⁽²⁾</i>	<i>Entropy (nats)</i>	OSPA⁽²⁾	OSPA⁽²⁾	<i>Loc (m)</i>	<i>OSPA⁽²⁾</i>
$N = 3$	V_1	50.00	2.50	47.50	0.269		47.70	8.32	39.38	0.071
	V_2	25.11	17.48	7.63	0.123		32.30	21.58	10.71	0.025
	V_{mo}	20.35	15.48	4.88	0.146		30.13	21.17	8.96	0.032
	V_{mo}^* (Ideal)	17.00	17.00	0.00	0.136		29.74	29.74	0.00	0.027
$N = 5$	V_1	50.00	0.83	49.17	0.271		48.95	1.45	47.50	0.073
	V_2	23.94	11.64	12.30	0.088		26.55	13.59	12.96	0.017
	V_{mo}	21.35	12.10	9.25	0.102		25.01	12.54	12.48	0.018
	V_{mo}^* (Ideal)	14.34	14.34	0.00	0.096		21.97	21.97	0.00	0.017
		Scenario 3 (Opposite)				Scenario 4 (Explosion)				
$N = 3$	V_1	35.50	6.13	29.38	0.246		39.30	2.67	36.63	0.297
	V_2	23.26	16.71	6.55	0.134		35.36	31.97	3.38	0.257
	V_{mo}	16.12	11.45	4.67	0.145		28.31	25.07	3.24	0.260
	V_{mo}^* (Ideal)	11.88	11.88	0.00	0.135		19.96	19.96	0.00	0.259
$N = 5$	V_1	45.57	3.07	42.50	0.238		36.39	8.89	27.50	0.290
	V_2	19.07	9.27	9.81	0.090		31.29	26.77	4.52	0.237
	V_{mo}	18.88	9.07	9.81	0.100		22.48	18.68	3.80	0.244
	V_{mo}^* (Ideal)	9.16	9.16	0.00	0.093		14.41	14.41	0.00	0.241

REFERENCES

[1] V. Cichella, I. Kammer, V. Dobrokhodov, and N. Hovakimyan, “Coordinated vision-based tracking for multiple UAVs,” in *Proceedings of 2015 IEEE/RSJ International Conference on Intelligent Robots and Systems (IROS)*, 2015, pp. 656–661.

[2] V. N. Dobrokhodov, I. I. Kammer, K. D. Jones, and R. Ghacheloo, “Vision-based tracking and motion estimation for moving targets using unmanned air vehicles,” *Journal of Guidance, Control, and Dynamics*, vol. 31, no. 4, pp. 907–917, 2008.

[3] L. Ma and N. Hovakimyan, “Cooperative target tracking in balanced circular formation: Multiple UAVs tracking a ground vehicle,” in *Proceedings of 2013 American Control Conference (ACC)*, 2013, pp. 5386–5391.

[4] J. Tisdale, A. Ryan, Zu Kim, D. Tornqvist, and J. K. Hedrick, “A multiple UAV system for vision-based search and localization,” in *Proceedings of 2008 American Control Conference (ACC)*, 2008, pp. 1985–1990.

[5] J. R. Bourne, M. N. Goodell, X. He, J. A. Steiner, and K. K. Leang, “Decentralized multi-agent information-theoretic control for target estimation and localization: Finding gas leaks,” *The International Journal of Robotics Research*, vol. 39, no. 13, pp. 1525–1548, 2020.

[6] J. R. Bourne, E. R. Pardyk, and K. K. Leang, “Coordinated Bayesian-based bioinspired plume source term estimation and source seeking for mobile robots,” *IEEE Transactions on Robotics*, vol. 35, no. 4, pp. 967–986, 2019.

[7] S. Gerasenko, A. Joshi, S. Rayaprolu, K. Ponnavaikko, and D. P. Agrawal, “Beacon signals: What, why, how, and where?” *Computer*, vol. 34, no. 10, pp. 108–110, 2001.

[8] R. R. Murphy, S. Tadokoro, D. Nardi, A. Jacoff, P. Fiorini, H. Choset, and A. M. Erkmen, “Search and rescue robotics,” in *Springer Handbook of Robotics*. Berlin, Heidelberg: Springer Berlin Heidelberg, 2008, pp. 1151–1173.

[9] R. Kays, S. Tilak, M. Crofoot, T. Fountain, D. Obando, A. Ortega, F. Kuemmeth, J. Mandel, G. Swenson, T. Lambert *et al.*, “Tracking animal location and activity with an automated radio telemetry system in a tropical rainforest,” *The Computer Journal*, vol. 54, no. 12, pp. 1931–1948, 2011.

[10] H. V. Nguyen, M. Chesser, L. P. Koh, H. Rezatofighi, and D. C. Ranasinghe, “TrackerBots: Autonomous unmanned aerial vehicle for real-time localization and tracking of multiple radio-tagged animals,” *Journal of Field Robotics*, vol. 36, no. 3, pp. 617–635, 2019.

[11] H. V. Nguyen, F. Chen, J. Chesser, H. Rezatofighi, and D. Ranasinghe, “LAVAPilot: Lightweight UAV trajectory planner with situational awareness for embedded autonomy to track and locate radio-tags,” in *Proceedings of 2020 IEEE/RSJ International Conference on Intelligent Robots and Systems (IROS)*, Oct 2020, pp. 2488–2495.

[12] B. Thomas, J. D. Holland, and E. O. Minot, “Wildlife tracking technology options and cost considerations,” *Wildlife Research*, vol. 38, no. 8, pp. 653–663, 2012.

[13] P. Zhu, L. Wen, D. Du, X. Bian, H. Fan, Q. Hu, and H. Ling, “Detection and tracking meet drones challenge,” *IEEE Transactions on Pattern Analysis and Machine Intelligence*, pp. 1–20, 2021.

[14] H.-T. Wai, Z. Yang, P. Z. Wang, and M. Hong, “Multi-agent reinforcement learning via double averaging primal-dual optimization,” in *Proceedings of the 32nd International Conference on Neural Information Processing Systems*, 2018, pp. 9649–9660.

[15] R. P. Mahler, *Advances in statistical multisource-multitarget information fusion*. Artech House, 2014.

[16] V. Roberge, M. Tarbouchi, and G. Labonté, “Comparison of parallel genetic algorithm and particle swarm optimization for real-time UAV path planning,” *IEEE Transactions on industrial informatics*, vol. 9, no. 1, pp. 132–141, 2012.

[17] L. C. MacDermed and C. L. Isbell, “Point based value iteration with optimal belief compression for Dec-POMDPs,” in *Proceedings of the 26th International Conference on Neural Information Processing Systems*, 2013, pp. 100–108.

[18] J. V. Messias, M. Spaan, and P. U. Lima, “Efficient offline communication policies for factored multiagent POMDPs,” in *Proceedings of the 24th International Conference on Neural Information Processing Systems*, 2011, pp. 1917–1925.

[19] D. Silver and J. Veness, “Monte-Carlo planning in large POMDPs,” in *Proceedings of the 23rd International Conference on Neural Information Processing Systems*, 2010, pp. 2164–2172.

[20] S. S. Baek, H. Kwon, J. A. Yoder, and D. Pack, “Optimal path planning of a target-following fixed-wing UAV using sequential decision processes,” in *Proceedings of 2013 IEEE/RSJ International Conference on Intelligent Robots and Systems*, 2013, pp. 2955–2962.

[21] S. Ragi and E. K. P. Chong, “UAV path planning in a dynamic environment via partially observable Markov decision process,” *IEEE*

Transactions on Aerospace and Electronic Systems, vol. 49, no. 4, pp. 2397–2412, 2013.

[22] D. S. Bernstein, R. Givan, N. Immerman, and S. Zilberstein, “The complexity of decentralized control of Markov decision processes,” *Mathematics of Operations Research*, vol. 27, no. 4, pp. 819–840, 2002.

[23] C. Amato and F. Oliehoek, “Scalable planning and learning for multiagent POMDPs,” in *Proceedings of the 29th AAAI Conference on Artificial Intelligence*, 2015, pp. 1995–2002.

[24] R. Nair, P. Varakantham, M. Tambe, and M. Yokoo, “Networked distributed POMDPs: A synthesis of distributed constraint optimization and POMDPs,” in *Proceedings of the 20th AAAI Conference on Artificial Intelligence*, vol. 5, 2005, pp. 133–139.

[25] Y. Rizk, M. Awad, and E. W. Tunstel, “Decision making in multiagent systems: A survey,” *IEEE Transactions on Cognitive and Developmental Systems*, vol. 10, no. 3, pp. 514–529, Sep. 2018.

[26] P. M. Dames and V. Kumar, “Autonomous localization of an unknown number of targets without data association using teams of mobile sensors,” *IEEE Transactions on Automation Science and Engineering*, vol. 12, no. 3, pp. 850–864, 2015.

[27] P. Dames, P. Tokekar, and V. Kumar, “Detecting, localizing, and tracking an unknown number of moving targets using a team of mobile robots,” *The International Journal of Robotics Research*, vol. 36, no. 13–14, pp. 1540–1553, 2017.

[28] X. Wang, R. Hoseinnezhad, A. K. Gostar, T. Rathnayake, B. Xu, and A. Bab-Hadiashar, “Multi-sensor control for multi-object Bayes filters,” *Signal Processing*, vol. 142, pp. 260–270, 2018.

[29] M. A. Beard, B.-T. Vo, B. N. Vo, and S. Arulampalam, “Void probabilities and Cauchy-Schwarz divergence for generalized labeled multi-Bernoulli models,” *IEEE Transactions on Signal Processing*, vol. 65, pp. 5047–5061, 2017.

[30] H. G. Hoang and B. T. Vo, “Sensor management for multi-target tracking via multi-Bernoulli filtering,” *Automatica*, vol. 50, no. 4, pp. 1135–1142, 2014.

[31] B. Ristic and B.-N. Vo, “Sensor control for multi-object state-space estimation using random finite sets,” *Automatica*, vol. 46, no. 11, pp. 1812 – 1818, 2010.

[32] Y. Sung and P. Tokekar, “GM-PHD filter for searching and tracking an unknown number of targets with a mobile sensor with limited FOV,” *IEEE Transactions on Automation Science and Engineering*, pp. 1–13, 2021.

[33] P. Bostrom-Rost, D. Axehill, and G. Hendeby, “Sensor management for search and track using the Poisson multi-Bernoulli mixture filter,” *IEEE Transactions on Aerospace and Electronic Systems*, vol. 57, no. 5, pp. 2771–2783, 2021.

[34] A. K. Gostar, R. Hoseinnezhad, and A. Bab-Hadiashar, “Multi-Bernoulli sensor-selection for multi-target tracking with unknown clutter and detection profiles,” *Signal Processing*, vol. 119, pp. 28 – 42, 2016.

[35] H. V. Nguyen, H. Rezatofighi, B.-N. Vo, and D. C. Ranasinghe, “Distributed Multi-object Tracking under Limited Field of View Sensors,” *IEEE Transactions on Signal Processing*, vol. 69, pp. 5329–5344, 2021.

[36] B. Charrow, N. Michael, and V. Kumar, “Active control strategies for discovering and localizing devices with range-only sensors,” in *Algorithmic Foundations of Robotics XI*. Springer, 2015, pp. 55–71.

[37] Y. Zhu, J. Wang, and S. Liang, “Multi-objective optimization based multi-Bernoulli sensor selection for multi-target tracking,” *Sensors*, vol. 19, no. 4, pp. 980 – 997, 2019.

[38] B. Vo, B. Vo, and M. Beard, “Multi-sensor multi-object tracking with the generalized labeled multi-bernoulli filter,” *IEEE Transactions on Signal Processing*, vol. 67, no. 23, pp. 5952–5967, Dec 2019.

[39] M. Piorkowski, N. Sarafijanovic-Djukic, and M. Grossglauser, “CRAW-DAD dataset epfl/mobility (v. 2009-02-24),” Downloaded from <https://crawdad.org/epfl/mobility/20090224>, Feb. 2009.

[40] H. V. Nguyen, H. Rezatofighi, B.-N. Vo, and D. C. Ranasinghe, “Multi-objective multi-agent planning for jointly discovering and tracking mobile objects,” in *Proceedings of the 34th AAAI Conference on Artificial Intelligence*. AAAI Press, Feb 2020, pp. 7227–7235.

[41] S. Thrun, W. Burgard, and D. Fox, *Probabilistic robotics*. MIT Press, 2005.

[42] B.-N. Vo, B.-T. Vo, and D. Phung, “Labeled random finite sets and the Bayes multi-target tracking filter,” *IEEE Transactions on Signal Processing*, vol. 62, no. 24, pp. 6554–6567, 2014.

[43] B.-T. Vo and B.-N. Vo, “Labeled random finite sets and multi-object conjugate priors,” *IEEE Transactions on Signal Processing*, vol. 61, no. 13, pp. 3460–3475, 2013.

[44] R. P. Mahler, *Statistical multisource-multitarget information fusion*. Artech House, 2007.

[45] R. Mahler, “A GLMB filter for unified multitarget multisensor management,” in *Signal Processing, Sensor/Information Fusion, and Target Recognition XXVIII*, vol. 11018. International Society for Optics and Photonics, 2019, p. 110180D.

[46] B.-N. Vo and B.-T. Vo, “A multi-scan labeled random finite set model for multi-object state estimation,” *IEEE Transactions on Signal Processing*, vol. 67, no. 19, pp. 4948–4963, 2019.

[47] S. Reuter, B.-T. Vo, B.-N. Vo, and K. Dietmayer, “The labeled multi-Bernoulli filter,” *IEEE Transactions on Signal Processing*, vol. 62, no. 12, pp. 3246–3260, 2014.

[48] M. Corah and N. Michael, “Distributed submodular maximization on partition matroids for planning on large sensor networks,” in *Proceedings of 2018 IEEE Conference on Decision and Control (CDC)*, 2018, pp. 6792–6799.

[49] R. Mahler, “Multitarget sensor management of dispersed mobile sensors,” in *Theory and Algorithms for Cooperative Systems*. World Scientific, 2004, pp. 239–310.

[50] T. M. Cover and J. A. Thomas, *Elements of information theory*. John Wiley & Sons, 2012.

[51] C. Geyer, “Likelihood inference for spatial point processes: Likelihood and computation,” in *Stochastic Geometry*. Chapman and Hall/CRC, 1999, pp. 141–172.

[52] J. Møller, *Statistical inference and simulation for spatial point processes*. Milton: Taylor & Francis Group, 2003.

[53] B.-N. Vo, S. Singh, and A. Doucet, “Sequential Monte Carlo methods for multitarget filtering with random finite sets,” *IEEE Transactions on Aerospace and Electronic Systems*, vol. 41, no. 4, pp. 1224–1245, 2005.

[54] U. Orguner and M. Demirekler, “Analysis of single Gaussian approximation of Gaussian mixtures in Bayesian filtering applied to mixed multiple-model estimation,” *International Journal of Control*, vol. 80, no. 6, pp. 952–967, 2007.

[55] G. L. Nemhauser, L. A. Wolsey, and M. L. Fisher, “An analysis of approximations for maximizing submodular set functions—I,” *Mathematical Programming*, vol. 14, no. 1, pp. 265–294, 1978.

[56] B. T. Vo, C. M. See, N. Ma, and W. T. Ng, “Multi-sensor joint detection and tracking with the Bernoulli filter,” *IEEE Transactions on Aerospace and Electronic Systems*, vol. 48, no. 2, pp. 1385–1402, 2012.

[57] S. Whiteson and D. M. Roijers, “Tutorial: Multi-objective planning under uncertainty,” *Proceedings of the 26th International Conference on Automated Planning and Scheduling*, 2016.

[58] A. Krause, H. B. McMahan, C. Guestrin, and A. Gupta, “Robust submodular observation selection,” *Journal of Machine Learning Research*, vol. 9, no. Dec, pp. 2761–2801, 2008.

[59] J. Koski, “Multicriterion structural optimization,” in *Optimization of Large Structural Systems*. Dordrecht: Springer Netherlands, 1993, pp. 793–809.

[60] C. A. C. Coello, G. B. Lamont, D. A. Van Veldhuizen *et al.*, *Evolutionary algorithms for solving multi-objective problems*. Springer, 2007, vol. 5.

[61] M. L. Fisher, G. L. Nemhauser, and L. A. Wolsey, “An analysis of approximations for maximizing submodular set functions—II,” in *Polyhedral combinatorics*. Springer, 1978, pp. 73–87.

[62] G. Calinescu, C. Chekuri, M. Pál, and J. Vondrák, “Maximizing a monotone submodular function subject to a matroid constraint,” *SIAM Journal on Computing*, vol. 40, no. 6, pp. 1740–1766, 2011.

[63] B.-T. Vo, B.-N. Vo, and A. Cantoni, “The cardinality balanced multi-target multi-Bernoulli filter and its implementations,” *IEEE Transactions on Signal Processing*, vol. 57, no. 2, pp. 409–423, 2008.

[64] G. Guido, V. Gallelli, D. Rogano, and A. Vitale, “Evaluating the accuracy of vehicle tracking data obtained from unmanned aerial vehicles,” *International Journal of Transportation Science and Technology*, vol. 5, no. 3, pp. 136–151, 2016.

[65] J. Zhu, K. Sun, S. Jia, Q. Li, X. Hou, W. Lin, B. Liu, and G. Qiu, “Urban traffic density estimation based on ultrahigh-resolution UAV video and deep neural network,” *IEEE Journal of Selected Topics in Applied Earth Observations and Remote Sensing*, vol. 11, no. 12, pp. 4968–4981, 2018.

[66] P. M. Dames, “Distributed multi-target search and tracking using the PHD filter,” *Autonomous robots*, vol. 44, no. 3, pp. 673–689, 2020.

[67] M. Beard, B. T. Vo, and B.-N. Vo, “A solution for large-scale multi-object tracking,” *IEEE Transactions on Signal Processing*, vol. 68, pp. 2754–2769, 2020.

[68] D. Schuhmacher, B.-T. Vo, and B.-N. Vo, “A consistent metric for performance evaluation of multi-object filters,” *IEEE Transactions on Signal Processing*, vol. 56, no. 8, pp. 3447–3457, 2008.